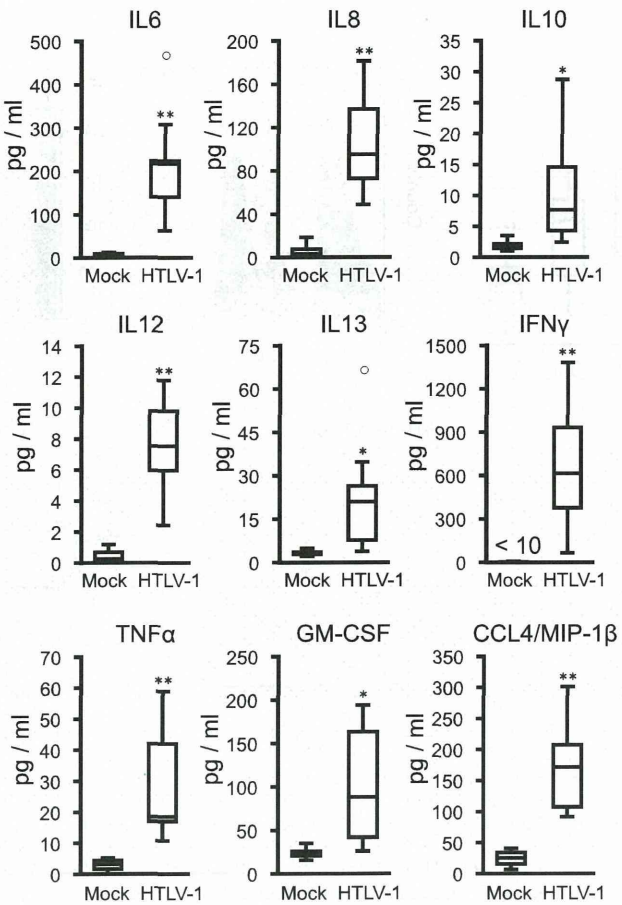

Figure 4. Induction of inflammatory cytokines in infected IBMI-huNOG mice. Human cytokine concentrations in plasma. Plasma was collected following sacrifice of mock-infected ($n = 4$) and HTLV-1–infected mice ($n = 8$). Seventeen cytokines were quantified using a cytokine bead array system. The concentrations of human IL-6, IL-8, IL-10, IL-12, IL-13, IFNγ, TNF-α, GM-CSF, and CCL4/MIP-1β are shown, all of which were significantly increased in the plasma of HTLV-1–infected mice. Increased expressions of the other 6 cytokines (IL-2, IL-4, IL-7, IL-17, G-CSF, and MCP-1) were also observed in infected mice but not statistically significant. On the other hand, little decrease in the concentrations of IL-1 and IL-5 was seen. Asterisks in each panel represent significant differences vs mock-infected mice (*$P < .05$, **$P < .01$ by Mann-Whitney U test).

human stem cells directly into the bone marrow cavity of NOD/Shi-SCID/IL-2Rγc null (NOG) mice using an IBMI method.

The efficacy of humanization achieved in this model is markedly superior to other procedures, such as intrahepatic or intravenous injection of human hematopoietic stem cells.[21,22,29] While T-lineage–cell populations become dominant over B-cell populations in the lymphoid organs of other humanized mouse systems within a few months after transplantation, in IBMI-huNOG mice the B-to-T-cell ratio remained constant for >8 months posttransplantation (Figure 1E). One possible explanation for this difference is that direct injection of hematopoietic stem cell preparations into the bone marrow of recipient mice improves the colonization efficiency of long-term stem cells.[27,46] Moreover, we used $CD133^+$ cells to generate IBMI-huNOG mice. CD133, the early hematopoietic progenitor cell marker, is thought to be ancestral to CD34 in human hematopoiesis.[47] Previous studies have revealed that $CD133^+$ cells were capable of differentiating not only into hematopoietic cells but also into endothelial, stromal, neuronal, and other type of cells.[47-49] It is possible that human mesenchymal stromal cells derived from $CD133^+$ cells support the development and maintenance of human B cells in the bone marrow microenvironment.

Having established a new humanized mouse model, we then infected IBMI-huNOG mice with HTLV-1 through inoculation with sublethally irradiated HTLV-1–producing cells.[28] HTLV-1–infected IBMI-huNOG mice recapitulated a large number of pathological features characteristic of ATL patients, including hyperproliferation of $CD3^+$ T cells, clonal proliferation of $CD25^+$ CD4 T cells, the appearance of flower cells in the periphery, hepatosplenomegaly, inflammatory hypercytokinemia, and down-regulation of CD3 on T cells.

Overgrowth of infected T cells was correlated with the expression of CD25 on CD4 T cells, consistent with recent reports.[17] However, the substantial proportion of $CD25^-$ CD4 T cells were also infected and identical T-cell clones, as determined by provirus integration site, were detected as the most abundant clones in both $CD25^-$ and $CD25^+$ CD4 T-cell populations, suggesting that CD25 expression likely occurs after infection in the course of clonal expansion. In addition, the expressions of *tax* and CD25 were inversely correlated. Further research will be necessary to identify molecular events associated with the suppression of *tax* expression in HTLV-1–infected $CD25^+$ CD4 T cells in relation to the development of ATL.

Banerjee et al[16] described the development of T-cell lymphoma following bone marrow transplantation of HTLV-1–infected $CD34^+/CD38^-$ hematopoietic stem cells into a NOD/SCID mouse. The lymphoma cells in these mice were capable of infiltrating into multiple organs but represented only $CD25^-$ or $CD25^{low}$ phenotypes. In contrast, HTLV-1–infected IBMI-huNOG mice developed leukemia in $CD25^+$ CD4 T cells, similar to that observed in ATL patients. The mechanism underlying this difference is unknown but may be due to differences in the developmental stage of T cells at the time of infection. Indeed, HTLV-1 infection in a different humanized mouse model, generated by intrahepatic transplantation of human $CD34^+$ stem cells into $Rag2^{-/-}\gamma c^{-/-}$ mice, induced formation of thymomas/lymphomas in mature CD4 T cells.[17] In this case, HTLV-1 infection was carried out 4 and 8 weeks after transplantation of $CD34^+$ hematopoietic stem cells, giving the human immune system time to develop. Thus the infection of $CD34^+$ stem cells per se does not appear to be sufficient for the induction of mature $CD25^+$ T cell malignancies and may require more developed lymphoid cells or a more appropriate microenvironment capable of supporting cell development.

Furthermore, HTLV-1–infected IBMI-huNOG mice almost exclusively developed leukemia, whereas HTLV-1 infection in the other humanized mouse models described above preferentially induced formation of lymphoma or thymoma. The reason for this difference is not clear but may stem from differences in the timing of T-cell infection. IBMI-huNOG mice were infected after the human hematopoietic system had been fully established, while in the other systems the infection was carried out before or shortly after stem cell transplantation.

In addition to leukemic growth of $CD25^+$ T cells, we also observed formation of flower cells in the peripheral blood of infected mice at later time points postinfection (>16 wpi). Although transformed T cells derived from Tax-transgenic mice were found to exhibit similar morphology,[15] none of the animal models described so far had recapitulated this pathology. Clonal analysis performed as part of this study demonstrated that the expansion of $CD25^+$ T-cell clones preceded the appearance of flower cells in periphery, suggesting a sequence of events that occurs during development of the malignancy. Thus, chronological

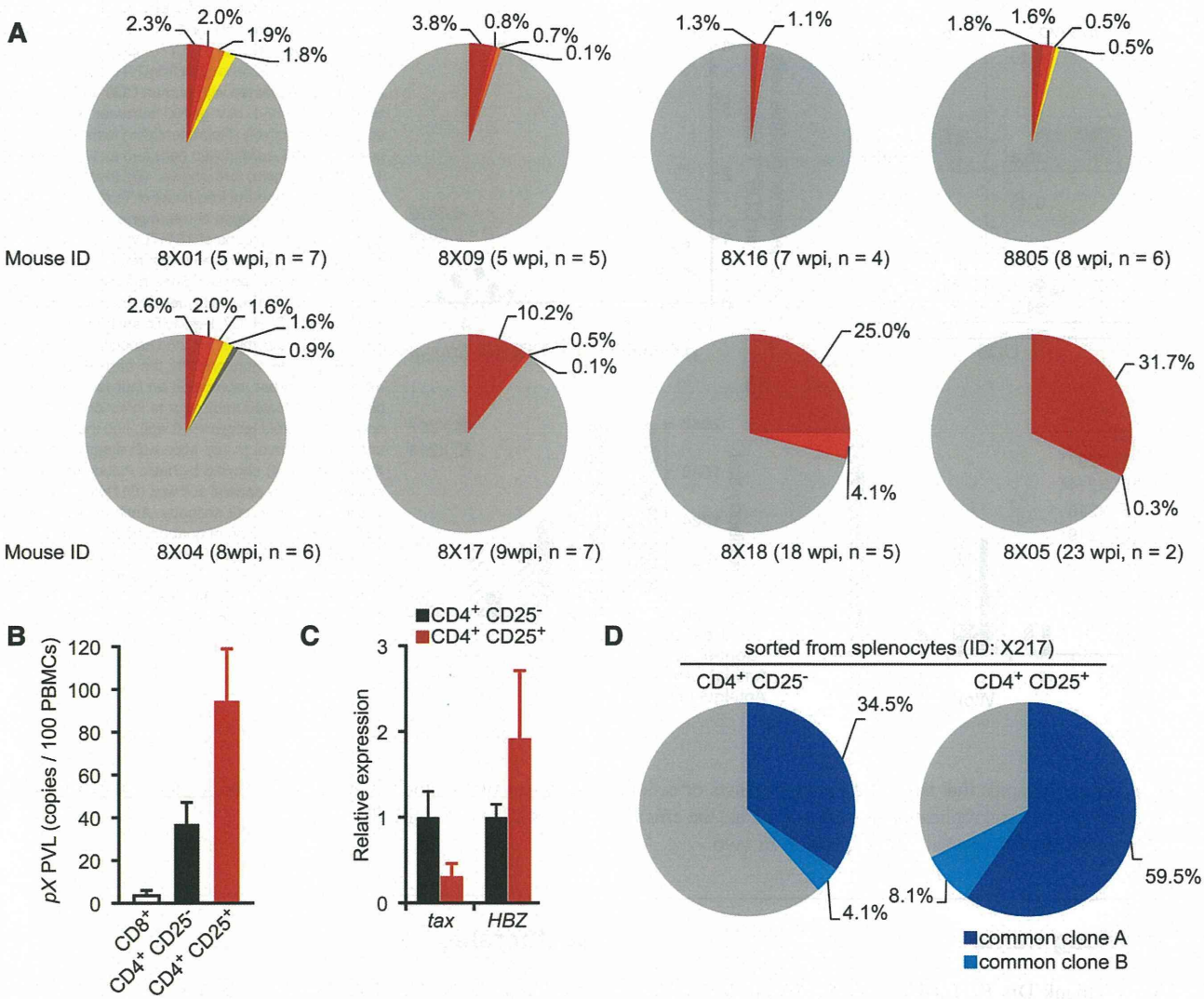

Figure 5. Progression of clonality in splenocytes of infected IBMI-huNOG. (A) Occupancy of HTLV-1–infected clones in the spleen. Abundant integration sites of HTLV-1 provirus were amplified by IL-PCR and subcloned into plasmids. The number of integration sites in each splenic DNA sample was determined by quantitative PCR using the clone-specific nucleotide sequence for each integration site. Results from 8 individual HTLV-1–infected mice are shown as pie charts. Size of the slice is proportional to the relative abundance of T-cell clones successfully amplified by IL-PCR, while data of minor clones with less than 0.1% occupancy were omitted. Gray regions represent clones with undefined integration sites. n, number of integration sites determined by nucleotide sequence of cloned PCR fragments in each mouse. (B) PVLs of specifiedT-cell populations. Splenocytes from HTLV-1–infected mice (n = 5) were sorted into $CD25^-$ or $CD25^+$ CD4 T cells and $CD8^+$ T cells. Genomic DNA isolated from each T-cell population was analyzed for PVL by real-time PCR using primers for the *pX* region of HTLV-1. (C) Comparative analysis of viral transcripts in $CD25^-$ and $CD25^+$ CD4 T-cell populations. Splenocytes from HTLV-1–infected mice (n = 5) are identical to those in mentioned above. The expression levels of *tax* (left) and *HBZ* (right) were analyzed by quantitative RT-PCR and were normalized to that of *HPRT1*. Results are presented as the fold change compared with the value in $CD25^-$ CD4 T cells. (D) Detection of common T-cell clones in the $CD25^-$ and $CD25^+$ CD4 T-cell populations. Clonal occupancy in both $CD25^-$ and $CD25^+$ populations are presented as pie charts. Two abundant common clones were analyzed for occupancy. Identified integration sites are listed in supplemental Table 5. The purity of each sorted population was >95% (supplemental Figure 3).

analysis of genetic and/or biochemical events in infected T cells from this mouse model should provide substantial information regarding the development of ATL.

We detected HLA-restricted CTLs against Tax protein of HTLV-1, as demonstrated in the peripheral blood of HTLV-1–infected carriers,[43] confirming the presence of an acquired immune response. Furthermore, the frequency of CTLs in CD8 T-cell populations were inversely correlated with the number of infected T cells in the spleen of humanized mice, similar to observations in HTLV-1–infected individuals.[43] The presence of functional T cells was also supported by the production of IgG antibodies specific to HTLV-1. Although humanized mice established by the transplantation of $CD34^+$ hematopoietic stem cells have been reported to produce antibodies against specific pathogens such as EBV,[22] HIV-1,[21] and DENV,[50] class switching from IgM to IgG was observed in only a few cases, likely due to immature T-cell development. In the IBMI-huNOG system, however, IgG production against HTLV-1 structural protein was observed after biphasic induction of antibodies after 8 weeks, indicating a functional interaction between CD4 T cells and B cells specific for viral antigens. Taken together, these data demonstrate induction of an adaptive immune response against HTLV-1 in HTLV-1–infected IBMI-huNOG mice, which may play an important role as selective pressure in the expansion of malignant T-cell clones.

In conclusion, our study demonstrates that the HTLV-1–infected IBMI-huNOG mouse represents a novel model that will facilitate elucidation of the molecular mechanism of in vivo development of ATL. Moreover, our model can also be used to develop and evaluate

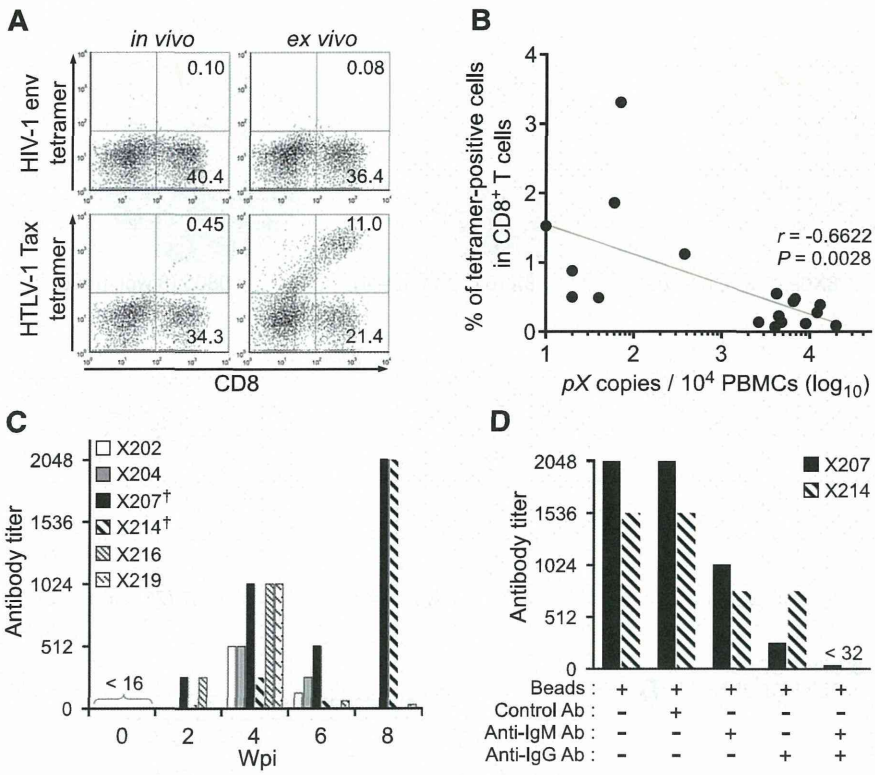

Figure 6. Induction of cellular and humoral immune responses against HTLV-1 in infected IBMI-huNOG mice. (A) Detection of HTLV-1–specific HLA-A*24:02-restricted CTLs. Splenocytes from HTLV-1–infected mice at 8 wpi were stained with human CD8 and Tax301-309 tetramer or HIV-1 env gp160 tetramer as a negative control, respectively. Representative results of tetramer-positive CD8 T cells in vivo (left) and ex vivo culture with Tax peptide (right) are shown. (B) Inverse correlation between PVL and the frequency of Tax301-309–specific CTLs. The percentages of tetramer-positive CD8 T cells and PVL in the spleens of 18 HTLV-1–infected mice are shown. One dot represents the result of an individual HTLV-1–infected mouse. Spearman's rank-correlation coefficient (r^2) was used to identify statistically significant correlations. (C) HTLV-1–specific antibody responses in HTLV-1–infected mice. HTLV-1–specific antibody titers in plasma were monitored by the particle agglutination method. Each bar represents an individual mouse. The plasma of indicated mice prior to infection were used as negative-controls (shown as 0 wpi), and these titers were undetectable level (<16). Mice with daggers (mouse ID: X207 and X214) showed biphasic induction of antibody responses; titers peaked at 8 wpi. (D) Detection of HTLV-1–specific IgM or IgG antibody. Antibody depletion was performed by addition of goat antibodies against human IgG or IgM and anti-goat antibody conjugated magnetic beads to the plasma of two mice, as shown in panel C (indicated by daggers). Bars represent antibody titers in the individual X207 and X214 mice. Ab, antibody.

novel preclinical therapies that target viral gene products or cellular molecules critical for viral replication as well as evaluate the efficacy of vaccine candidates to prevent viral expansion in vivo.

Acknowledgments

The authors thank Drs R. Tatsumi and Y. Adachi for advice in establishing humanized mice and assistance with the pathological analysis, respectively. The authors are grateful to the Japanese Red Cross Kinki Cord Blood Bank for providing the samples used in this study.

This work was supported by Grants-in-Aid for Scientific Research C from the Ministry of Education, Culture, Sports, Science and Technology of Japan (grants 21590515 and 24590562) (J.F.); a MEXT-Supported Program for the Strategic Research Foundation at Private Universities; and Health and Labour Sciences Research Grants for Research on Emerging and Re-emerging Infectious Diseases from Ministry of Health, Labour and Welfare (grant 24171601) (T.U.) (grant 23211801) (M. Tanaka).

Authorship

Contribution: K.T. and J.F. designed the research; K.T. and R.X. established and maintained humanized mice; K.T., R.X., M. Tei and T.U. carried out experiments; M. Tanaka was involved in the IL-PCR analysis; K.T., R.X., M. Tei, and J.F. analyzed results; N.T. performed statistical analysis; K.T. designed the figures; and K.T. and J.F. wrote the paper.

Conflict-of-interest disclosure: The authors declare no competing financial interests.

Correspondence: Jun-ichi Fujisawa, Department of Microbiology, Kansai Medical University, 2-5-1 Shin-machi, Hirakata, Osaka 573-1010, Japan; e-mail: fujisawa@hirakata.kmu.ac.jp.

References

1. Hinuma Y, Nagata K, Hanaoka M, et al. Adult T-cell leukemia: antigen in an ATL cell line and detection of antibodies to the antigen in human sera. *Proc Natl Acad Sci USA.* 1981;78(10):6476-6480.
2. Poiesz BJ, Ruscetti FW, Gazdar AF, Bunn PA, Minna JD, Gallo RC. Detection and isolation of type C retrovirus particles from fresh and cultured lymphocytes of a patient with cutaneous T-cell lymphoma. *Proc Natl Acad Sci USA.* 1980;77(12):7415-7419.
3. Osame M, Usuku K, Izumo S, et al. HTLV-I associated myelopathy, a new clinical entity. *Lancet.* 1986;1(8488):1031-1032.
4. Kondo T, Kono H, Miyamoto N, et al. Age- and sex-specific cumulative rate and risk of ATLL for HTLV-I carriers. *Int J Cancer.* 1989;43(6):1061-1064.
5. Boxus M, Twizere JC, Legros S, Dewulf JF, Kettmann R, Willems L. The HTLV-1 Tax interactome. *Retrovirology.* 2008;5:76.
6. Matsuoka M, Jeang KT. Human T-cell leukemia virus type 1 (HTLV-1) and leukemic transformation: viral infectivity, Tax, HBZ and therapy. *Oncogene.* 2011;30(12):1379-1389.
7. Yoshida M, Seiki M, Yamaguchi K, Takatsuki K. Monoclonal integration of human T-cell leukemia provirus in all primary tumors of adult T-cell leukemia suggests causative role of human T-cell leukemia virus in the disease. *Proc Natl Acad Sci USA.* 1984;81(8):2534-2537.
8. Shimoyama M, Minato K, Tobinai K, et al. Atypical adult T-cell leukemia-lymphoma: diverse clinical manifestations of adult T-cell leukemia-lymphoma. *Jpn J Clin Oncol.* 1983;13(Suppl 2):165-187.
9. Okayama A, Tachibana N, Ishihara S, et al. Increased expression of interleukin-2 receptor alpha on peripheral blood mononuclear cells in HTLV-I tax/rex mRNA-positive asymptomatic carriers. *J Acquir Immune Defic Syndr Hum Retrovirol.* 1997;15(1):70-75.

10. Bieberich CJ, King CM, Tinkle BT, Jay G. A transgenic model of transactivation by the Tax protein of HTLV-I. *Virology.* 1993;196(1):309-318.
11. Feuer G, Zack JA, Harrington WJ Jr, et al. Establishment of human T-cell leukemia virus type I T-cell lymphomas in severe combined immunodeficient mice. *Blood.* 1993;82(3): 722-731.
12. Kondo A, Imada K, Hattori T, et al. A model of in vivo cell proliferation of adult T-cell leukemia. *Blood.* 1993;82(8):2501-2509.
13. Furuta RA, Sugiura K, Kawakita S, Inada T, Ikehara S, Matsuda T, Fujisawa J. Mouse model for the equilibration interaction between the host immune system and human T-cell leukemia virus type 1 gene expression. *J Virol.* 2002;76(6): 2703-2713.
14. Dewan MZ, Terashima K, Taruishi M, et al. Rapid tumor formation of human T-cell leukemia virus type 1-infected cell lines in novel NOD-SCID/ gammac(null) mice: suppression by an inhibitor against NF-kappaB. *J Virol.* 2003;77(9): 5286-5294.
15. Hasegawa H, Sawa H, Lewis MJ, et al. Thymus-derived leukemia-lymphoma in mice transgenic for the Tax gene of human T-lymphotropic virus type I. *Nat Med.* 2006;12(4):466-472.
16. Banerjee P, Tripp A, Lairmore MD, et al. Adult T-cell leukemia/lymphoma development in HTLV-1-infected humanized SCID mice. *Blood.* 2010;115(13):2640-2648.
17. Villaudy J, Wencker M, Gadot N, et al. HTLV-1 propels thymic human T cell development in "human immune system" Rag2$^{-/-}$ gamma c$^{-/-}$ mice. *PLoS Pathog.* 2011;7(9):e1002231.
18. Satou Y, Yasunaga J, Zhao T, et al. HTLV-1 bZIP factor induces T-cell lymphoma and systemic inflammation in vivo. *PLoS Pathog.* 2011;7(2): e1001274.
19. Kazanji M. HTLV type 1 infection in squirrel monkeys (Saimiri sciureus): a promising animal model for HTLV type 1 human infection. *AIDS Res Hum Retroviruses.* 2000;16(16):1741-1746.
20. Lairmore MD, Silverman L, Ratner L. Animal models for human T-lymphotropic virus type 1 (HTLV-1) infection and transformation. *Oncogene.* 2005;24(39):6005-6015.
21. Watanabe S, Terashima K, Ohta S, et al. Hematopoietic stem cell-engrafted NOD/SCID/ IL2Rgamma null mice develop human lymphoid systems and induce long-lasting HIV-1 infection with specific humoral immune responses. *Blood.* 2007;109(1):212-218.
22. Yajima M, Imadome K, Nakagawa A, et al. A new humanized mouse model of Epstein-Barr virus infection that reproduces persistent infection, lymphoproliferative disorder, and cell-mediated and humoral immune responses. *J Infect Dis.* 2008;198(5):673-682.
23. Hasegawa A, Ohashi T, Hanabuchi S, Kato H, Takemura F, Masuda T, Kannagi M. Expansion of human T-cell leukemia virus type 1 (HTLV-1) reservoir in orally infected rats: inverse correlation with HTLV-1-specific cellular immune response. *J Virol.* 2003;77(5):2956-2963.
24. Kannagi M, Hasegawa A, Kinpara S, Shimizu Y, Takamori A, Utsunomiya A. Double control systems for human T-cell leukemia virus type 1 by innate and acquired immunity. *Cancer Sci.* 2011; 102(4):670-676.
25. Ito M, Hiramatsu H, Kobayashi K, et al. NOD/SCID/gamma(c)(null) mouse: an excellent recipient mouse model for engraftment of human cells. *Blood.* 2002;100(9):3175-3182.
26. Kushida T, Inaba M, Hisha H, et al. Intra-bone marrow injection of allogeneic bone marrow cells: a powerful new strategy for treatment of intractable autoimmune diseases in MRL/lpr mice. *Blood.* 2001;97(10):3292-3299.
27. Wang J, Kimura T, Asada R, et al. SCID-repopulating cell activity of human cord blood-derived CD34- cells assured by intra-bone marrow injection. *Blood.* 2003;101(8):2924-2931.
28. Miyoshi I, Kubonishi I, Yoshimoto S, et al. Type C virus particles in a cord T-cell line derived by co-cultivating normal human cord leukocytes and human leukaemic T cells. *Nature.* 1981; 294(5843):770-771.
29. Nie C, Sato K, Misawa N, et al. Selective infection of CD4+ effector memory T lymphocytes leads to preferential depletion of memory T lymphocytes in R5 HIV-1-infected humanized NOD/SCID/IL-2Rgammanull mice. *Virology.* 2009;394(1):64-72.
30. Takamori A, Hasegawa A, Utsunomiya A, et al. Functional impairment of Tax-specific but not cytomegalovirus-specific CD8+ T lymphocytes in a minor population of asymptomatic human T-cell leukemia virus type 1-carriers. *Retrovirology.* 2011;8:100.
31. Ueno S, Umeki K, Takajo I, et al. Proviral loads of human T-lymphotropic virus Type 1 in asymptomatic carriers with different infection routes. *Int J Cancer.* 2012;130(10):2318-2326.
32. Etoh K, Tamiya S, Yamaguchi K, et al. Persistent clonal proliferation of human T-lymphotropic virus type I-infected cells in vivo. *Cancer Res.* 1997; 57(21):4862-4867.
33. Umeki K, Hisada M, Maloney EM, Hanchard B, Okayama A. Proviral loads and clonal expansion of HTLV-1-infected cells following vertical transmission: a 10-year follow-up of children in Jamaica. *Intervirology.* 2009;52(3):115-122.
34. Hiramatsu H, Nishikomori R, Heike T, Ito M, Kobayashi K, Katamura K, Nakahata T. Complete reconstitution of human lymphocytes from cord blood CD34+ cells using the NOD/SCID/ gammacnull mice model. *Blood.* 2003;102(3): 873-880.
35. Nitta T, Tanaka M, Sun B, Hanai S, Miwa M. The genetic background as a determinant of human T-cell leukemia virus type 1 proviral load. *Biochem Biophys Res Commun.* 2003;309(1):161-165.
36. Yamano Y, Araya N, Sato T, et al. Abnormally high levels of virus-infected IFN-gamma+ CCR4+ CD4+ CD25+ T cells in a retrovirus-associated neuroinflammatory disorder. *PLoS ONE.* 2009;4(8):e6517.
37. Matsuda M, Maeda Y, Shirakawa C, et al. CD3 down-regulating factor in sera and culture supernatants of leukaemic cells from patients with adult T cell leukaemia. *Br J Haematol.* 1993;83(2): 212-217.
38. Yamada Y, Ohmoto Y, Hata T, et al. Features of the cytokines secreted by adult T cell leukemia (ATL) cells. *Leuk Lymphoma.* 1996;21(5-6): 443-447.
39. Chiba K, Hashino S, Izumiyama K, Toyoshima N, Suzuki S, Kurosawa M, Asaka M. Multiple osteolytic bone lesions with high serum levels of interleukin-6 and CCL chemokines in a patient with adult T cell leukemia. *Int J Lab Hematol.* 2009;31(3):368-371.
40. Chen J, Petrus M, Bryant BR, et al. Autocrine/ paracrine cytokine stimulation of leukemic cell proliferation in smoldering and chronic adult T-cell leukemia. *Blood.* 2010;116(26):5948-5956.
41. Ohshima K, Mukai Y, Shiraki H, Suzumiya J, Tashiro K, Kikuchi M. Clonal integration and expression of human T-cell lymphotropic virus type I in carriers detected by polymerase chain reaction and inverse PCR. *Am J Hematol.* 1997; 54(4):306-312.
42. Kurihara K, Harashima N, Hanabuchi S, et al. Potential immunogenicity of adult T cell leukemia cells in vivo. *Int J Cancer.* 2005;114(2):257-267.
43. Akimoto M, Kozako T, Sawada T, et al. Anti-HTLV-1 tax antibody and tax-specific cytotoxic T lymphocyte are associated with a reduction in HTLV-1 proviral load in asymptomatic carriers. *J Med Virol.* 2007;79(7):977-986.
44. Harashima N, Kurihara K, Utsunomiya A, et al. Graft-versus-Tax response in adult T-cell leukemia patients after hematopoietic stem cell transplantation. *Cancer Res.* 2004;64(1):391-399.
45. Kozako T, Arima N, Toji S, et al. Reduced frequency, diversity, and function of human T cell leukemia virus type 1-specific CD8+ T cell in adult T cell leukemia patients. *J Immunol.* 2006; 177(8):5718-5726.
46. Nakamura K, Inaba M, Sugiura K, Yoshimura T, Kwon AH, Kamiyama Y, Ikehara S. Enhancement of allogeneic hematopoietic stem cell engraftment and prevention of GVHD by intra-bone marrow bone marrow transplantation plus donor lymphocyte infusion. *Stem Cells.* 2004; 22(2):125-134.
47. Jaatinen T, Hemmoranta H, Hautaniemi S, et al. Global gene expression profile of human cord blood-derived CD133+ cells. *Stem Cells.* 2006; 24(3):631-641.
48. Herrera MB, Bruno S, Buttiglieri S, et al. Isolation and characterization of a stem cell population from adult human liver. *Stem Cells.* 2006;24(12): 2840-2850.
49. Martin-Rendon E, Hale SJ, Ryan D, et al. Transcriptional profiling of human cord blood CD133+ and cultured bone marrow mesenchymal stem cells in response to hypoxia. *Stem Cells.* 2007;25(4):1003-1012.
50. Kuruvilla JG, Troyer RM, Devi S, Akkina R. Dengue virus infection and immune response in humanized RAG2($^{-/-}$)gamma(c)($^{-/-}$) (RAG-hu) mice. *Virology.* 2007;369(1):143-152.

OPEN

Citation: Blood Cancer Journal (2013) 3, e132; doi:10.1038/bcj.2013.30

www.nature.com/bcj

ORIGINAL ARTICLE

Oral administration of an HSP90 inhibitor, 17-DMAG, intervenes tumor-cell infiltration into multiple organs and improves survival period for ATL model mice

E Ikebe[1], A Kawaguchi[2,3,13], K Tezuka[4,13], S Taguchi[1,13], S Hirose[1], T Matsumoto[1], T Mitsui[1], K Senba[1], A Nishizono[1], M Hori[5], H Hasegawa[6], Y Yamada[6], T Ueno[4], Y Tanaka[7], H Sawa[3], W Hall[8], Y Minami[9], KT Jeang[10], M Ogata[11], K Morishita[12], H Hasegawa[2], J Fujisawa[4] and H Iha[1]

In the peripheral blood leukocytes (PBLs) from the carriers of the human T-lymphotropic virus type-1 (HTLV-1) or the patients with adult T-cell leukemia (ATL), nuclear factor kappaB (NF-κB)-mediated antiapoptotic signals are constitutively activated primarily by the HTLV-1-encoded oncoprotein Tax. Tax interacts with the I κB kinase regulatory subunit NEMO (NF-κB essential modulator) to activate NF-κB, and this interaction is maintained in part by a molecular chaperone, heat-shock protein 90 (HSP90), and its co-chaperone cell division cycle 37 (CDC37). The antibiotic geldanamycin (GA) inhibits HSP90's ATP binding for its proper interaction with client proteins. Administration of a novel water-soluble and less toxic GA derivative, 17-dimethylaminoethylamino-17-demethoxygeldanamycin hydrochloride (17-DMAG), to Tax-expressing ATL-transformed cell lines, C8166 and MT4, induced significant degradation of Tax. 17-DMAG also facilitated growth arrest and cellular apoptosis to C8166 and MT4 and other ATL cell lines, although this treatment has no apparent effects on normal PBLs. 17-DMAG also downregulated Tax-mediated intracellular signals including the activation of NF-κB, activator protein 1 or HTLV-1 long terminal repeat in Tax-transfected HEK293 cells. Oral administration of 17-DMAG to ATL model mice xenografted with lymphomatous transgenic Lck-Tax (Lck proximal promoter-driven Tax transgene) cells or HTLV-1-producing tumor cells dramatically attenuated aggressive infiltration into multiple organs, inhibited *de novo* viral production and improved survival period. These observations identified 17-DMAG as a promising candidate for the prevention of ATL progression.

Blood Cancer Journal (2013) **3,** e132; doi:10.1038/bcj.2013.30; published online 16 August 2013

Keywords: 17-DMAG; molecular chaperon; Tax; ATL; apoptosis; transgenic model

INTRODUCTION

Nuclear factor kappaB (NF-κB) is a transcription factor that regulates immune and antiapoptotic responses to multiple extracellular stresses.[1,2] Under normal conditions, most NF-κB molecules are sequestered in the cytoplasm by the inhibitor I κB. In response to cellular stress, I κB is rapidly phosphorylated by the NF-κB activator I κB kinase (IKK) and ubiquitylated for degradation by the proteasome. This frees NF-κB for translocation into the nucleus, where it directs the transcriptional activation of NF-κB-responsive genes.[3,4] IKK is comprised of three different subunits, IKKα, IKKβ and IKKγ/NEMO (NF-κB essential modulator). IKKγ is also known as NF-κB essential modulator (NEMO). NEMO trimerizes rapidly in response to extracellular stimuli, such as the pro-inflammatory cytokine tumor necrosis factor-α (TNF-α), and recruits the two catalytic subunits, IKKα/β, to form a highly phosphorylated active IKK holoenzyme.[5] Several genetic studies have shown that cytokine-triggered activation of what is termed the canonical NF-κB activation pathway is primarily dependent on NEMO and IKKβ,[6,7] whereas IKKα activity is required for the development of the skin, limbs and lymph nodes.[8,9] Upon stimulation, several accessory proteins are recruited to IKK, and the molecular size of this active IKK complex reaches more than 1 MDa.[10,11] The molecular chaperone heat-shock protein 90 (HSP90) and its co-chaperone cell division cycle 37 (CDC37) are components of this high molecular weight (HMW)-IKK complex, and they play crucial roles in maintaining the activity of the complex.[12] The antibiotic geldanamycin (GA) specifically binds to the ATPase domain of HSP90 and inhibits its function as a molecular chaperone, resulting in the efficient inhibition of TNF-α-mediated activation of NF-κB.[12,13]

The human T-lymphotropic virus type-1 (HTLV-1), which is the etiologic agent of adult T-cell leukemia (ATL), encodes the oncoprotein Tax.[14–16] Tax activates NF-κB by interacting

[1]Department of Infectious Diseases, Faculty of Medicine, Oita University, Yufu, Japan; [2]Department of Pathology, National Institute of Infectious Diseases, Musashimurayama, Japan; [3]Department of Molecular Pathobiology, 21st Century COE Program for Zoonosis Control, Hokkaido University Research Center for Zoonosis Control, Sapporo, Japan; [4]Department of Microbiology, Kansai Medical University, Moriguchi, Japan; [5]Department of Hematology, Ibaraki Prefectural Central Hospital, Kasama, Ibaraki, Japan; [6]Department of Laboratory Medicine, Nagasaki University Graduate School of Biomedical Sciences, Nagasaki, Japan; [7]Department of Immunology, Graduate School of Medicine, University of the Ryukyus, Nishihara, Japan; [8]Department of Medical Microbiology, Centre for Research in Infectious Diseases, Conway Institute of Biomolecular and Biomedical Research, University College Dublin, Dublin, Ireland; [9]Department of Biotechnology, Maebashi Institute of Technology, Maebashi, Japan; [10]Molecular Virology Section, Laboratory of Molecular Microbiology, National Institute of Allergy and Infectious Diseases, Bethesda, MD, USA; [11]Department of Hematology, Faculty of Medicine, Oita University, Yufu, Japan and [12]Division of Tumor and Cellular Biochemistry, Department of Medical Sciences, Faculty of Medicine, University of Miyazaki, Miyazaki, Japan. Correspondence: Dr H Iha, Department of Infectious Diseases, Faculty of Medicine, Oita University, 1-1 Idaigaoka, Hasama, Yufu, Oita 879-5593, Japan.
E-mail: hiha@oita-u.ac.jp
[13]These authors contributed equally to this work.
Received 25 June 2012; revised 24 June 2013; accepted 28 June 2013

physically with NEMO.[10,17] NF-κB activation mediated by this Tax–NEMO interaction is similar to that of the TNF-α-triggered 'canonical' pathway. Tax induces IKK phosphorylation, ubiquitylation and proteasome-dependent degradation of I κB, thereby inducing the translocation of NF-κB into the nucleus.[18,19] However, in contrast to the TNF-α-triggered canonical pathway, which is transient and mostly IKKβ dependent, Tax-mediated NF-κB activation is persistent and utilizes both the IKKα and IKKβ subunits.[20,21] From these observations, we speculated that oncogenic Tax-mediated activation of NF-κB is distinguishable from the canonical NF-κB activation pathway, and indeed, we have succeeded in inhibiting Tax-mediated NF-κB activation using selected sets of NEMO-mutant peptides.[11]

Those earlier studies led us to ask whether GA can inhibit Tax-mediated HMW-IKK formation and suppress NF-κB activation as has been demonstrated in the TNF-α-triggered canonical pathway. To address this, we treated ATL cell lines or HEK293 cells transfected with a Tax expression vector with GA or its less toxic derivative 17-dimethylaminoethylamino-17-demethoxygeldanamycin hydrochloride (17-DMAG).[22] We found that these HSP90 inhibitors downregulated Tax-mediated intracellular activity including the activation of NF-κB, activator protein 1 and HTLV-1 long terminal repeat (HTLV-1-LTR). These findings prompted us to investigate the molecular mechanisms by which HSP90 inhibitors disrupt Tax-mediated signaling in ATL cells. We found that the stability of Tax in ATL cells is heavily dependent on the HSP90/CDC37 chaperones and that Tax is rapidly degraded without these chaperones following the addition of HSP90 inhibitors. Apoptosis of ATL cells was also induced by GA and 17-DMAG. Finally, the oral administration of 17-DMAG to severe combined immunodeficient (SCID) mice transplanted with lymphomatous cells bearing Lck proximal promoter-driven Tax transgene (Lck-Tax) cells[23] markedly inhibited the aggressive infiltration of these Lck-Tax cells into multiple organs. The same procedure to the humanized NOG (huNOG) mice inoculated with HTLV-1-producing Jurkat cells also resulted in the suppression of *de novo* viral production and improved the survival period.

MATERIALS AND METHODS

Ethics statement

This study was carried out in strict accordance with the recommendations in the Guidelines for Proper Conduct of Animal Experiments, Science Council of Japan (http://www.scj.go.jp/en/animal/index.html). All procedures involving animals and their care were approved by the Animal Care Committee of Oita University, National Institute of Infectious Diseases and Kansai Medical University in accordance with the Regulations for Animal Experiments in Oita University (approval ID: 24-22).

Chemicals, cells and cell culture conditions

All chemicals used in this study including 17-DMAG[22] and cell lines or peripheral blood leukocytes (PBLs) were described in Supplementary Information.

Coimmunoprecipitation and immunoblot

One million cells of MT4 and C8166 treated with or without 17-DMAG and HEK293 cells transfected with each plasmid (maximum 1 μg) by FugeneHD (Roche Applied Science, Tokyo, Japan) for 40 h were lysed with coimmunoprecipitation (Co-IP) buffer. Each 200 μg of precleared (with 30 μl of protein G agarose, CalBiochem, Millipore Corporation, Billerica, MA, USA) lysates was incubated with 2 μg of rabbit polyclonal anti-HSP90 (Stressgen Bioreagents, Ann Arbor, MI, USA) or rabbit anti-FLAG antibody (Sigma-Aldrich, St Louis, MO, USA) for at least 3 h at 4° C. Antibody–protein G complexes were washed, resolved by sodium dodecyl sulfate-polyacrylamide gel electrophoresis and transferred onto a polyvinylidene difluoride membrane, and specific proteins were detected by monoclonal anti-Tax, -HSP90 (Stressgen), -Flag, -tubulin (Sigma) or polyclonal anti-IKKb (Cell Signaling Technology) antibodies, respectively.

Real-time quantitative reverse transcriptase-PCR by the LightCycler system

Total RNA from MT4 cells treated with or without 17-DMAG was isolated using ISOGEN (Wako Pure Chemical Industries, Ltd., Osaka, Japan), and contaminated DNA was removed. cDNA was constructed by the Thermoscript reverse transcriptase-PCR system (Invitrogen, Life Technologies Japan Co., Tokyo, Japan), and real-time quantitative PCRs for Tax and glucose-6-phosphate 1-dehydrogenase were performed on a Roche LC480 system (Roche) with indicated probe and primer sets.

Cell viability assay

Cell lines or PBLs from ATL patients or healthy donors were treated with 2.5 μM of 17-DMAG for 1–4 days. After every 24 h incubation, cell viabilities were counted with Cell Counting Kit (Dojindo Laboratories, Kumamoto, Japan).

Caspase-3/7 assay

Cells used in the 'cell viability assay' were also subjected for apoptosis activity with cappase-3/7 assay and GLOMAX 96 microplate luminometer (Promega KK, Tokyo, Japan).

Plasmids

The details of plasmid pSG5-Tax,[24] HSP90,[25] Cdc37,[26] CMV-Tax or LTR-Tax[11] and CoralHue-Tax or −CDC37 vectors (MBL Co. Ltd., Nagoya, Japan)[27] are described in Supplementary Information.

Luciferase assay

HEK293 cells were transfected with plasmid DNA mixture containing the reporter plasmids (NF-κB-Luc or HTLV-1-LTR-Luc[11] and RSV-β-galactosidase as a transfection indicator) and Tax expression vectors (pSG5-Tax, CMV-Tax or LTR-Tax) by FugeneHD. After 24 h incubation of the transfection, where indicated, 17-DMAG at concentrations listed in the figures was added, and cells were further incubated for 16 h. Cell lysates were subjected to the luciferase assay kit and GLOMAX 96.

Microscopic observation of cells

HEK293 cells were transfected with phmKGN-MC-Tax and phmKGC-MN-Cdc37 or its mutant −Cdc37(N200) or −Cdc37(N180) for 48 h and then treated with 1 μM of Hoechst 34442 (Sigma). Light and fluorescent (green fluorescent protein (GFP) or Hoechst 34442) microscopic observation and photography were performed by BZ-9000 Biorevo (Keyence Co. Ltd., Osaka, Japan).

Transfer of Lck-Tax transgenic cells to SCID mice and treatment with 17-DMAG

SCID mice were injected intraperitoneally with 2×10^6 Lck-Tax cells.[23] 17-DMAG was administered orally 5 days per week, with 5, 15 or 30 mg/kg for 2–3 weeks, and then mice were sacrificed for pathological examination.

HTLV-1 infection to huNOG and flow cytometric analysis of peripheral bloods

Suspension of irradiated 1×10^6 HTLV-1-producing JEX cells was inoculated intraperitoneally into huNOG mice[28] at the age between 24 and 28 weeks. Peripheral blood cells were routinely collected every 2 weeks after infection. Spleen, bone marrow and lymph node were collected, and PBLs were stained with florescent dye-conjugated antibodies against human cellular surface markers.

DNA isolation and quantification of proviral load

Genomic DNA was extracted from single cell suspension of tissue or peripheral blood followed by the conventional phenol extraction method. Proviral load was measured by quantitative PCR as previously described.[29]

Histopathological examination and immunohistochemistry

Tissues were directly fixed in the neutral buffered formalin (Sigma), embedded in paraffin, sectioned and stained with hematoxylin and eosin. Peripheral blood smears were prepared using Giemsa staining and examined by light microscopy.

For details, see Supplementary Information.

RESULTS

The NF-κB-activating Tax–HSP90–IKK ternary complex is disaggregated by HSP90 inhibitors that induce Tax degradation

The molecular chaperone HSP90 and its co-chaperone CDC37 are both recruited to IKK and play essential roles in TNF-α-triggered HMW-IKK formation and subsequent NF-κB activation. The addition of the HSP90-specific inhibitor GA completely suppresses NF-κB signaling.[12] As we previously demonstrated that the expression of Tax also resulted in the formation of a HMW-IKK complex for activating NF-κB,[11] we speculated that the inhibition of HSP90 function by GA would also affect Tax-mediated NF-κB signaling. First, using Tax-expressing MT4 cells, we confirmed the interaction of Tax with HSP90 in the same protein complex by Co-IP assays (Figure 1a). We then treated MT4 cells for 24 h with a newly developed, less toxic and water-soluble GA derivative, 17-DMAG,[22] to evaluate its effects on the formation of a Tax-induced ternary complex, Tax–HSP90–IKK. To our surprise, the amount of Tax in MT4 cells decreased progressively with increasing doses of 17-DMAG (Figure 1b, upper panel) despite no apparent changes in the amount of HSP90 in the same lysate (data not shown). Under these conditions, the interaction between HSP90 and IKKβ was clearly reduced with increasing doses of 17-DMAG (Figure 1b, middle panel), whereas the amount of HSP90 immunoprecipitated throughout this range of concentrations was unchanged (Figure 1b, lower panel).

We then examined the kinetics of Tax degradation in MT4 cells treated with 17-DMAG. Reductions in Tax levels were observed in cells treated for 12 h and continued over time until by 48 h, when the level of Tax became undetectable (Figure 1c). This 17-DMAG-induced Tax degradation stabilized I κBα, whereas another NF-κB inhibitor dexamethasone had no effects (Supplementary Figure 1). Tax degradation by 17-DMAG occurred prior to mRNA suppression as the marked decrease of Tax mRNA was not observed until 24 h after treatment (Figure 1d), whereas protein level of Tax was obviously decreased by 12 h (compare Figures 1c and d). Our previous study indicated that Tax degradation is partly induced by caspase,[30] and polyubiquitylation had little effects on its cellular stability.[31] We therefore re-evaluated which pathway is responsible for the 17-DMAG-induced Tax degradation (Figure 1e). Tax degradation was partly blocked by the caspase inhibitor zVAD-fmk[30] and by autophagy inhibitors 3-methyladenine (3-MA) and 5-aminoimidazole-4-carboxamide-1-b-D-ribofuranoside (AICAR)[32] but not by the proteasome inhibitor MG132. Similar findings were obtained from parallel studies using another ATL cell line, C8166 (data not shown), although more investigation is needed for fully understanding of Tax instability.

GA and its derivatives are known to suppress a variety of intracellular signaling pathways, including NF-κB activation by inhibiting IKK.[12,33] One of the most important functions of NF-κB is to protect cells from apoptotic stress. A portion of 2.5 μM of 17-DMAG is sufficient to induce Tax degradation (Figure 1c) and I κBα stabilization (Supplementary Figure 1), which implies the suppression of ATL cell growth; however, it is important to know whether this concentration is toxic to normal PBLs. We, therefore, confirmed the median inhibitory concentrations of 17-DMAG for several ATL or non-ATL cell lines along with normal PBLs.

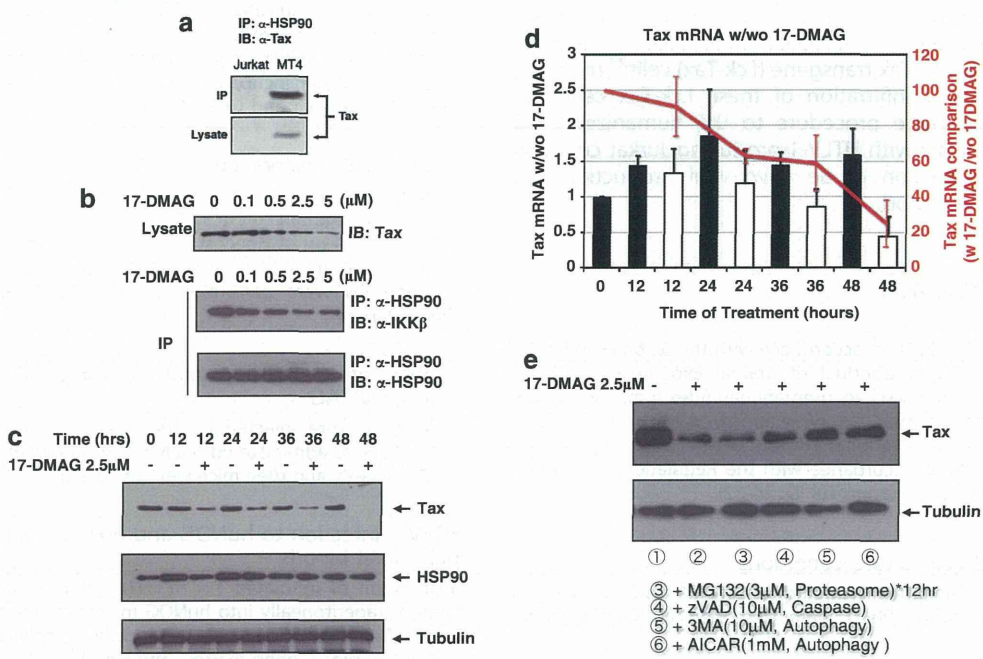

Figure 1. 17-DMAG inhibits HSP90–Tax–IKK ternary complex formation and induces Tax degradation in ATL cells. (**a**) Co-IP of Tax and HSP90. Four million Jurkat or MT4 cells were lysed with Co-IP buffer, and 50 μg total of cell lysates were subjected to IP with 2 μg of rabbit polyclonal anti-HSP90 antibody, followed by immunoblot (IB) with mouse monoclonal anti-Tax antibody (upper panel). The amount of expressed Tax in each cell line was verified by IB with anti-Tax against 10 μg of cell lysates (lower panel). (**b**) 17-DMAG's effects on Tax expression level and physical interaction between HSP90 and IKKβ in MT4 cells. Four million MT4 cells were treated with the indicated concentrations of 17-DMAG for 16 h. Co-IP and IB against immunoprecipitates or lysates were carried out as in panel **a**. (**c**) Ten micrograms of each cell lysate from MT4 cells treated with or without 2.5 μM of 17-DMAG for the indicated periods were subjected to sodium dodecyl sulfate-polyacrylamide gel electrophoresis, and Tax (upper panel), HSP90 (middle panel) or tubulin (lower panel) expression was detected using monoclonal anti-Tax, anti-HSP90 or anti-tubulin antibodies. (**d**) Expression levels of Tax in 17-DMAG-treated MT4 cells. mRNAs were prepared from the same aliquots of MT4 cells described in panel **c**. mRNAs from 17-DMAG-untreated fractions (black bars) and 17-DMAG-treated fractions (2.5 μM, white bars) with indicated time courses were analyzed with the universal probes (Roche) and primers through the LightCycler PCR method according to the manufacturer's direction. Comparison of Tax mRNAs with or without 17-DMAG was also indicated with a red line graph as a division of Tax mRNA with 17-DMAG/without 17-DMAG at each time point. (**e**) Four million MT4 cells were treated with 2.5 μM 17-DMAG for 24 h (lanes 2–6) and then additional 3 μM MG132 for 12 h (lane 3), 10 μM zVAD-fmk (lane 4) and 3-MA (lane 5) and 1 mM AICAR (lane 6) for 24 h. Lysates were prepared for IB of Tax and tubulin.

The median inhibitory concentrations to ATL cells vary from 0.06 to 2.33 μM, which is much lower than that of non-ATL Jurkat cells (9.32 μM), and three PBLs did not show any significant growth suppression with 10 μM of 17-DMAG (Supplementary Figure 2). We set the concentration of 17-DMAG at 2.5 μM and measured the effects on the viability of ATL cells (cell lines established from ATL patients' PBLs or cord blood cocultured with ATL patients' PBLs or primary PBLs of ATL patients) and other leukemic cells, as well as PBLs from HTLV-1-negative controls. Most of the ATL cell lines treated with 17-DMAG exhibited a rapid decrease in viability, whereas normal PBLs were unaffected by the drug (Figure 2a). 17-DMAG treatment also resulted in a marked increase in caspase-3/7 activity in most of the ATL cell lines while having no significant caspase perturbation in control PBLs (Figure 2b).

Downregulation of Tax occurs at the post-transcriptional stage

We then proceeded to examine the details of 17-DMAG-dependent inhibitory effects on the Tax–HSP90–IKK ternary complex by transfection of two different Tax expression vectors into HEK293 cells. One was driven by the simian virus 40 early promoter and

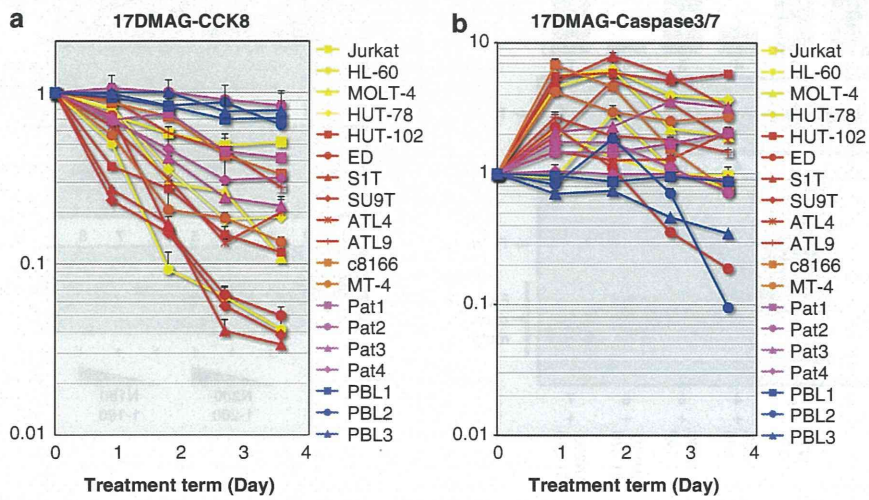

Figure 2. 17-DMAG induces growth arrest and apoptosis in ATL cells. Two million cells from each ATL cell line established from ATL patients' PBLs (HUT-102, ED, S1T, SU9T, ATL4 and ATL9; red lines), ATL cell lines established by coculture of cord blood and ATL patients' PBLs (C8166 and MT4; orange lines), PBLs from ATL patients (Pat1 to Pat4; purple lines), non-ATL leukemic cell lines (Jurkat, HL-60, MOLT-4 and HUT-78; yellow lines) or healthy donors (PBL1, PBL2 and PBL3; blue lines) were treated with 2.5 μM of 17-DMAG for 1–4 days. After each 24 h incubation, 10^4 (**a**) or 5×10^3 (**b**) cells were transferred to each well of a 96-well plate. (**a**) One-tenth volume of Cell Counting Kit 8 solution (Dojindo) was added to each fraction. Thirty minutes after incubation, the absorbance at 465 nm was measured using an E-max precision microplate reader (Molecular Devices Japan Co. Ltd., Tokyo, Japan). (**b**) The same volume of Apo-ONE homogeneous Caspase-3/7 assay solution was added to cells, and chemical luminescence was quantified with GloMax luminometer (Promega).

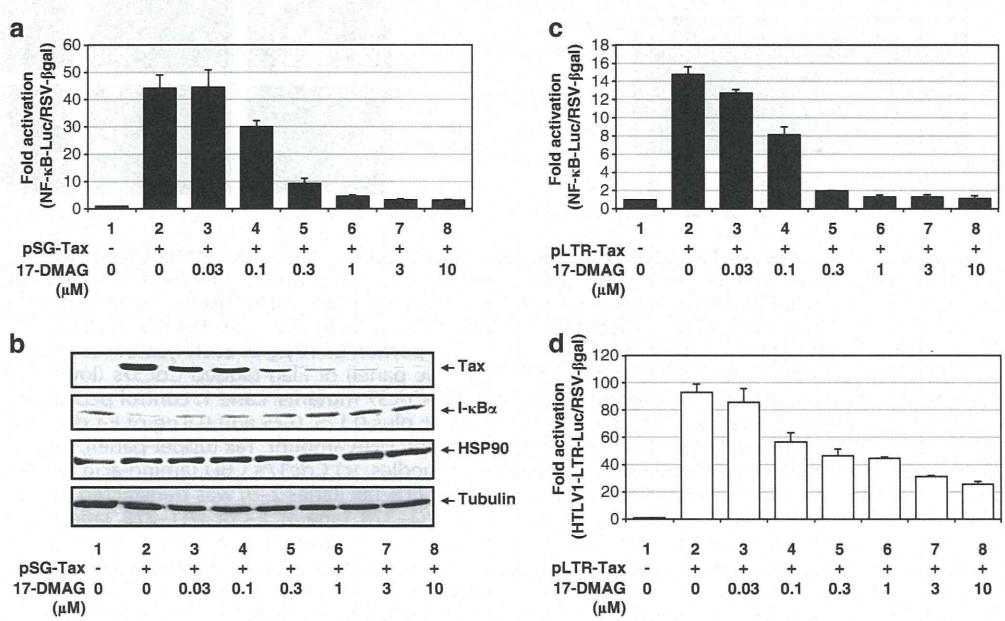

Figure 3. 17-DMAG downregulates all the Tax-mediated signaling in HEK293 cells. Fifty thousand HEK293 cells in each well on a 12-well plate were transfected with 0.5 μg of pSG-Tax (**a**, **c**) or pLTR-Tax along with 50 ng of NF-κB-luciferase (**a**, **c**) or HTLV-1-LTR-luciferase (**d**) and 50 ng of RSV-β-galactosidase control plasmid. A portion of 0.1–5 μM of 17-DMAG was added as indicated for 16 h. (**b**) The expression levels of Tax, HSP90 and tubulin in 10 μg of lysates from panel (**a**) were monitored by IB with monoclonal antibodies for each protein.

β-globin intron II (pSG5-Tax),[24] whereas the other was driven by the HTLV-1-LTR (LTR-Tax). These lines were transfected with either a NF-κB-responsive or a HTLV-1-LTR luciferase reporter (Figures 3a and b and Figures 3c and d, respectively) and RSV-β-galactosidase for readout normalization. 17-DMAG treatment was found to suppress Tax-mediated NF-κB (Figures 3a, b and c) or HTLV-1-LTR activation (Figure 3d) regardless of whether Tax was expressed from pSG5-Tax (Figures 3a and b) or LTR-Tax (Figures 3c and d). In these experiments, the ectopically expressed Tax from transfected plasmid was again downregulated by 17-DMAG (Figure 3b). The same results were also obtained from the cell lysates transfected with LTR-Tax or CMV-Tax (data not shown). In addition to these two enhancers, activator protein 1 activation by Tax[34] was also inhibited by 17-DMAG (data not shown). As the three discrete pathways

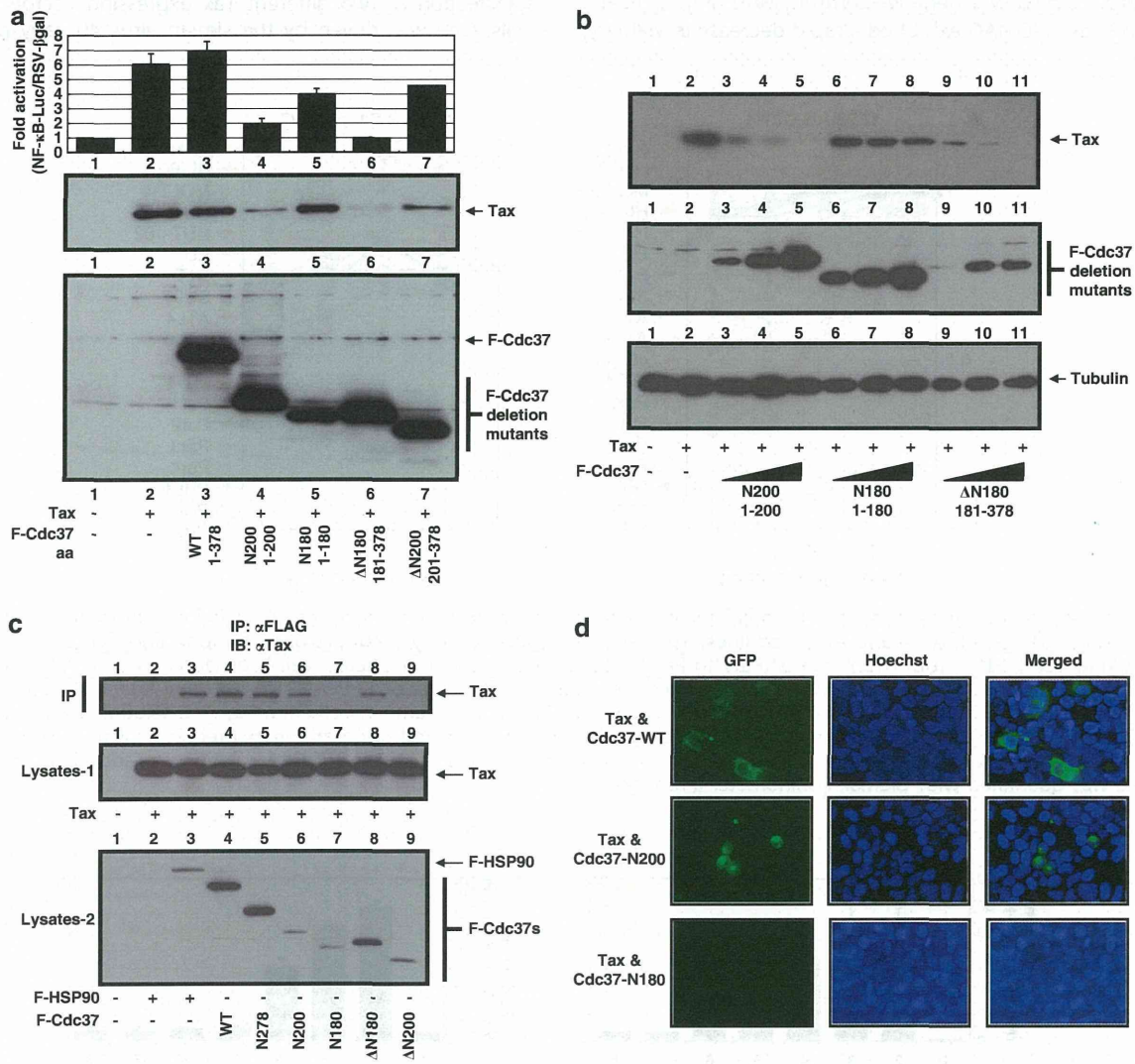

Figure 4. CBD of Cdc37 plays a crucial role for Tax stability in cells. (**a**) Co-transfection of LTR-Tax and pcDNA3-Flag-tagged Cdc37 (F-Cdc37) mutants. Lane 1: control pcDNA3 1 μg; lane 2: LTR-Tax 0.5 μg + pcDNA3 0.5 μg; lane 3: LTR-Tax 0.5 μg + F-Cdc37(1–378) wild type 0.5 μg; lane 4: LTR-Tax 0.5 μg + F-Cdc37(1–200) 0.5 μg; lane 5: LTR-Tax 0.5 μg + F-Cdc37(1–180) 0.5 μg; lane 6: LTR-Tax 0.5 μg + F-Cdc37(181–378) 0.5 μg; lane 7: LTR-Tax 0.5 μg + F-Cdc37(201–378) 0.5 μg. After 40 h transfection, HEK293 cells were lysed with 100 μl of lysis buffer, and the NF-κB-dependent luciferase activity was normalized with β-galactosidase value (upper panel). A portion of 10 μg of each lysate was resolved by sodium dodecyl sulfate-polyacrylamide gel electrophoresis, and the expression of Tax (middle panel) or Flag-tagged Cdc37s (lower panel) was detected by specific monoclonal antibodies. (**b**) Dose-dependent degradation of Tax by F-Cdc37 mutants. Lane 1: control pcDNA3 1 μg; lanes 2–11: 0.5 μg of LTR-Tax; lanes 3–5: plus 0.125, 0.25 and 0.5 μg of F-Cdc37(1–200); lanes 6–8: plus 0.125, 0.25 and 0.5 μg of F-Cdc37(1–180); lanes 9–11: plus 0.125, 0.25 and 0.5 μg of F-Cdc37(181–378). pcDNA3 was added to normalize the DNA amount. Tax (upper panel), Flag-tagged Cdc37s (middle panel) and tubulin (lower panel) were detected by specific monoclonal antibodies. (**c**) Cdc37's CBD (amino-acid residues 181–200(ref. 26)) is required for Tax interaction. A portion of 0.5 μg of control pcDNA3 (lane 1) or LTR-Tax (lanes 2–9) was transfected (lysate-1, middle panel) and 0.5 g of control pcDNA3 (lanes 1 and 2), F-HSP90 (lane 3), wild-type F-Cdc37(1–378, lane 4), F-Cdc37(1–278, lane 5), F-Cdc37(1–200, lane 6), F-Cdc37(1–180, lane 7), F-Cdc37(181–378, lane 8) and F-Cdc37(201–378, lane 9) were transfected separately (lysate-2, lower panel). The expression of each protein in cell lysates was detected by specific monoclonal antibodies (middle and bottom panels). A portion of 200 μg of each lane's cell lysates was mixed and subjected to Co-IP with 2 μg of rabbit anti-Flag antibodies, and each Co-IP complex was washed four times with Co-IP buffer, and following sodium dodecyl sulfate-polyacrylamide gel electrophoresis, Tax was detected by anti-Tax antibody (upper panel). (**d**) GFP two-hybrid binding assay between Cdc37 and Tax. HEK293 cells seeded on the six-well plates were transfected with phmKGN-MC-Tax and phmKGC-MN-Cdc37 or its mutant −Cdc37(N200) and −Cdc37(N180) by FugeneHD. After 48 h incubation, the transfected HEK293 cells were treated with Hoechst 34442 (Sigma) at the final concentration of 1 μM. Light and fluorescent (GFP and Hoechst 34442) microscopic observation and photography were performed by BZ-9000 Biorevo all-in-one fluorescence microscope (Keyence).

activated by Tax are inhibited by 17-DMAG treatment, the simplest interpretation suggests that all these effects arise from 17-DMAG-mediated destabilization of the Tax protein itself.

The client-binding domain of CDC37 plays crucial roles in Tax stabilization and Tax-mediated NF-κB activation

The molecular chaperone activity of HSP90 is usually exerted in cooperation with various co-chaperones. CDC37 was identified along with HSP90 as an essential component for a TNF-α-activated HMW-IKK complex.[12] As our current study shows the involvement of HSP90 in Tax-mediated HMW-IKK formation and NF-κB activation,[11,17] we generated Flag-tagged serial deletion mutants of HSP90 and CDC37 to examine their potential effects on Tax activity.

HSP90 has three distinct functional domains as described in Supplementary Figure 3.[35–37] We generated five deletion mutants, N, N+M, M, M+C and C, and transduced each with a Tax expression vector into HEK293 cells to determine any dominant-negative effects. Surprisingly, none of these mutants showed suppressive effects on Tax-mediated NF-κB activation or Tax stabilization (data not shown).

We then investigated the possible involvement of CDC37 in Tax stabilization and NF-κB signaling according to its functional domains (Supplementary Figure 3), namely, an HSP90-binding domain expanding through M164 to E221;[38] a kinase-binding domain at amino-acid residues 40–110;[39] a client-binding domain (CBD, amino-acid residues 181–200);[26] and a self-dimerization domain (amino-acid residues 240–260).[39] Although overexpression of full-length CDC37 slightly enhanced NF-κB activation (Figure 4a upper panel, lane 3), the mutants containing CBD, CDC37(1–200) and CDC37(181–378), strongly suppressed Tax-mediated NF-κB activation (Figure 4a upper panel, lanes 4 and 6) and induced extensive Tax degradation (Figure 4a middle panel, lanes 4 and 6). The mutants CDC37(1–180) and CDC37 (201–378) lacking CBD had little effects on either NF-κB activation or Tax stability (lanes 5 and 7). Tax degradation was reconfirmed by titration of these mutants (Figure 4b). Both CCD37(1–200) and CCD37 (181–378) progressively promoted Tax degradation (lanes 3–5 and 9–11, respectively), but CDC37(1–180) had little effects (lanes 6–8). Coexpression of certain sets of CDC37 mutants could promote Tax degradation through impaired physical interaction with Tax. We transfected HEK293 cells with Tax or Flag-CDC37 expression vectors separately to avoid spontaneous Tax degradation, and each cell lysate was mixed and applied for Co-IP experiments with anti-Flag antibodies (Figure 4c). Each protein expression was confirmed by immunoblotting for Tax (middle panel) or Flag (lower panel). Although the immunoprecipitates from wild-type HSP90 (upper panel, lane 3), CDC37 (lane 4) and Tax-degrading CDC37(1–200) and CDC37(181–378) (lanes 6 and 8) contained Tax in the complex, the immunoprecipitates from CDC37(1–180) and CDC37(201–378) lacking Tax-degrading properties did not (lanes 7 and 9).

Finally, we examined direct interaction between the two proteins using a GFP two-hybrid assay. Tax, tagged with the N-terminal portion of Kusabira-Green[27] fluorescent protein, and CDC37s (1–378, 1–200 and 1–180), tagged with the C-terminal portion, were co-transfected into HEK293 cells. Consistent with Co-IP results, co-transfectants of Tax and CDC37(1–378) or CDC37(1–200) emitted green fluorescence but Tax plus CDC37

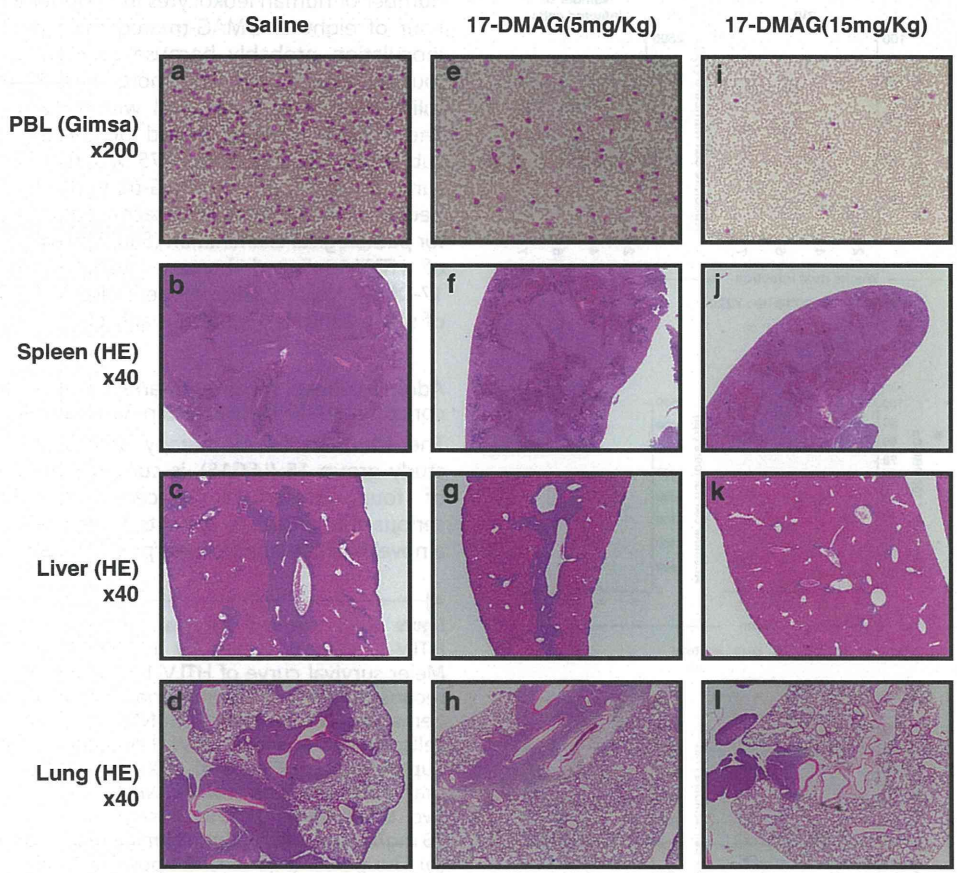

Figure 5. Oral administration of 17-DMAG blocks aggressive infiltration of Lck-Tax Tg cells into multiple organs of SCID mice. Two million Lck-Tax Tg cells were injected intraperitoneally into SCID mice. 17-DMAG was administered orally 5 days per week, with 5 mg/kg body weight (**e**–**h**) or 15 mg/kg body weight (**i**–**l**) or untreated (**a**–**d**). Mice were sacrificed after 21 days incubation, and organs were processed for Giemsa (**a**, **e**, **i**) or hematoxylin and eosin (HE, **b**–**d**, **f**–**h** and **j**–**l**) staining. Microscopic observations were performed and photographed with indicated magnifications. Tg, transgenic.

(1–180) did not. The Tax–CDC37(1–200) complex was translocated to the nucleus, whereas Tax–CDC37(1–378; wild type) stayed in the cytoplasm (Figure 4d). Collectively, these findings suggested the direct involvement of CDC37 for Tax stabilization.

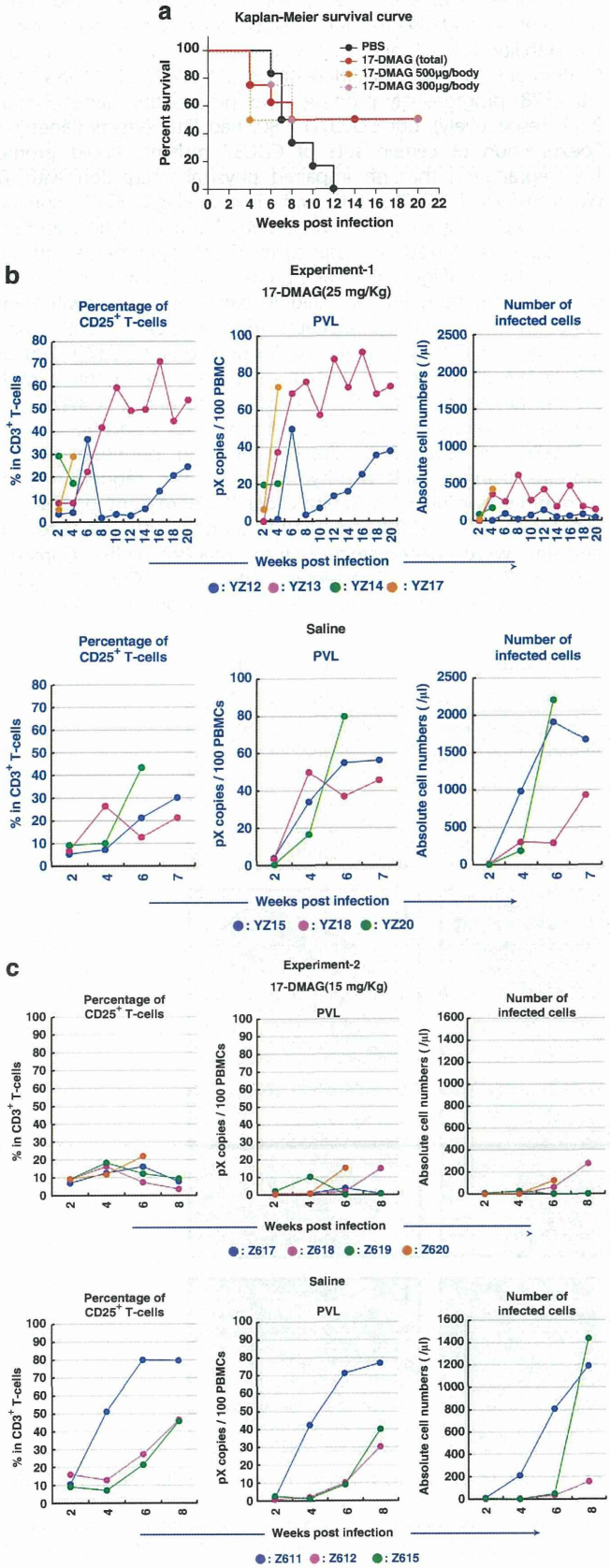

An oral administration of 17-DMAG to ATL model mice induced blockade of aggressive proliferation and multiple tissue invasions of transformed lymphocytes and improved survival rate

The demonstration that 17-DMAG has profound effects on Tax stability and the fact that it is water soluble suggested that this compound could be tested in a recently developed preclinical model of ATL.[23,28]

SCID mice were injected with 2×10^6 Lck-Tax cells intraperitoneally and treated for 5 consecutive days per week for 2 weeks with saline alone or with 17-DMAG in saline at 5 or 15 mg/kg. Mice were euthanized 21 days after cell inoculation. The blood smear indicated apparent reduction of Lck-Tax cells with increasing doses of 17-DMAG to saline controls (Figures 5a, e and i), although the quantitative cell counts were not obtained. The white pulp in greatly enlarged spleens (splenomegaly) of control mice was markedly expanded with red pulp compression (Figure 5b), and the livers and lungs of saline control mice were characterized by extensive perivascular infiltrations with Lck-Tax cells (Figures 5c and d). These pathologies were progressively reduced in mice treated with 17-DMAG (spleen, Figures 5f and j; liver, Figures 5g and k; and lung, Figures 5h and l).

We then determined the survival improvement through 17-DMAG oral administration with another preclinical ATL model (Figure 6). Each 7 (14 in total) huNOG mice[28] were injected with 1×10^6 HTLV-1-producing JEX cells (details are described in Supplementary Information), and 2 weeks after inoculation, each 4 of these mice (8 in total) were treated 20 times with 15 or 25 mg/kg of 17-DMAG for 4 weeks (as shown in Supplementary Figure 4), whereas the remaining 6 mice received saline only. The percentage of CD25-positive T cells, proviral load and the number of human leukocytes in peripheral blood were monitored. Four of eight 17-DMAG-treated mice died within 8 weeks post inoculation probably because of high drug dosage, but other four mice (50%) survived more than 20 weeks, whereas all the saline-treated controls died within 12 weeks post inoculation. The average survival period of controls and 17-DMAG-treated subjects were 8.33 and 14.75 weeks, respectively. However, the survival periods of 17-DMAG-treated subjects could be extended because four subjects were sacrificed at 24 weeks post inoculation for pathological examination (Supplementary Figure 4). The numbers of HTLV-1-infected human leukocytes in peripheral blood of 17-DMAG-treated subjects were also 5–10 times fewer than those of saline controls (Figures 6b and c).

Additive effects for growth arrest and apoptosis induction by concomitant 17-DMAG/Nutlin-3a treatment against ATL cells

The standard chemotherapy against ATL, named as leukemia study group 15 (LSG15), is currently employing the combination of four different anticancer drugs that frequently brings serious side effects to patients.[40] We previously demonstrated that a novel MDM-2-antagonizing/p53-stabilizing drug, Nutlin-3a, induces

Figure 6. Improved survival and suppression of the growth of HTLV-1-infected T cells by 17-DMAG oral treatment. (**a**) Kaplan–Meier survival curve of HTLV-1-infected huNOG mice. All mice have reconstituted human immune system by the transplantation of hematopoietic stem cells (huNOG) and have received 1 million JEX cells, which produce HTVL-1 infectious virus (see the details in Supplementary Figure 4). JEX/huNOG mice received 17-DMAG by oral administration for 4 weeks (2–6 weeks post inoculation, five times/week) at the dosage of 25 mg/kg (orange line) and 15 mg/kg (pink line). Control mice received the same volume of PBS. (**b**) The percentage of CD25-positive T cells, PVL and the number of HTLV-1-infected cells in peripheral blood of infected mice are shown. Upper panel represents the results from 17-DMAG-treated (25 mg/kg) mice; lower panel represents those of control mice. (**c**) Same experiments with 17-DMAG (15 mg/kg, upper panel) and PBS control (lower panel). PBS, phosphate buffered saline; PVL, proviral load.

the senescent death to ATL cells.[41] We then examined the additive anti-ATL effects of 17-DMAG and Nutlin-3a. Suboptimal dose of 17-DMAG (0.1 μM) or Nutlin-3a (1 μM) alone did not induce sufficient apoptotic or growth-arrest activities to ATL cell lines. However, the combined use of both induced significant growth suppressive and apoptotic properties (Figure 7), suggesting the possible combinational use of these drugs for further clinical studies.

DISCUSSION

HTLV-1 is the etiologic agent of ATL. Current studies indicate that worldwide there are more than 20 million HTLV-1 carriers and that 5% of these carriers will develop ATL.[42] The current standard for treatment of acute- or lymphoma-type ATL in Japan is CHOP or its modified regimen LSG15; however, the responses to this treatment regimen are limited to 31.1% of patients with 2-year survivals.[40] As malignant cells from relapsed patients are also resistant to other chemotherapeutic interventions, novel strategies for treatment of ATL are urgently required.

In this study, we demonstrated the significant inhibitory effects of 17-DMAG on Tax-mediated NF-κB signaling *in vitro* and *ex vivo*. The most striking observations obtained *in vitro* were (a) 17-DMAG-induced Tax degradation that resulted from inhibiting the formation of the Tax–IKK–HSP90/CDC37 ternary complex (Figures 1a–d); (b) induction of growth suppression and apoptosis of ATL cells while having little or no effect on normal PBLs (Figures 2a and b). We also found that the stability of Tax was heavily dependent on the CBD of CDC37 (Figures 4a and b). GA-dependent NF-κB downregulation in ATL cells was reported, and inhibition of autophagic activity seemed to affect the conversion of p100 (NF-κB2 precursor) to active p52.[32] We observed this time 17-DMAG-dependent Tax degradation and its blockade by AICAR and 3-MA (autophagy inhibitors) but not by the proteasome inhibitor MG-132 (Figure 1d), suggesting the direct involvement of the autophagosome on Tax metabolism in cells. This issue should further be investigated with ubiquitylation-deficient mutants Tax[24,31] or the autophagy-deficient cells.[43,44]

The CBD of CDC37 has been reported to bind preferentially to a specific glycine-rich motif — GXGXXG.[45] Indeed, Tax has a similar motif in its N terminus. CBD played crucial roles in stabilizing Tax and Tax–CDC37 complex formation (Figures 4c and d). CBD-containing mutants of CDC37 seemed to enhance the machinery responsible for Tax degradation as we did not detect any decrease in Tax levels in response to an siRNA knockdown of CDC37 (Supplementary Figure 5). Interestingly, the Tax-destabilizing CDC37(N200) translocated Tax to the nucleus, whereas wild-type CDC37 stayed with Tax in the cytoplasm (Figure 4d), and it implies that this translocation could be related to the Tax destabilization. For the future, it would be worth trying to identify a chemical compound that mimics the structure of CBD and could function as an inducer of Tax degradation. HSP90 and its co-chaperone's involvement in multiple signaling cascades, especially, in cancer cells, has been reported.[46,47] Indeed, 17-DMAG also suppressed NF-κB signaling mediated by other activators NIK, MEKK1, AKT, TAB2 and IKKα/β (data not shown). We also found that 17-DMAG treatment induced Tax degradation; potentially 17-DMAG treatment may also have led to the destabilization of other NF-κB signaling activators.

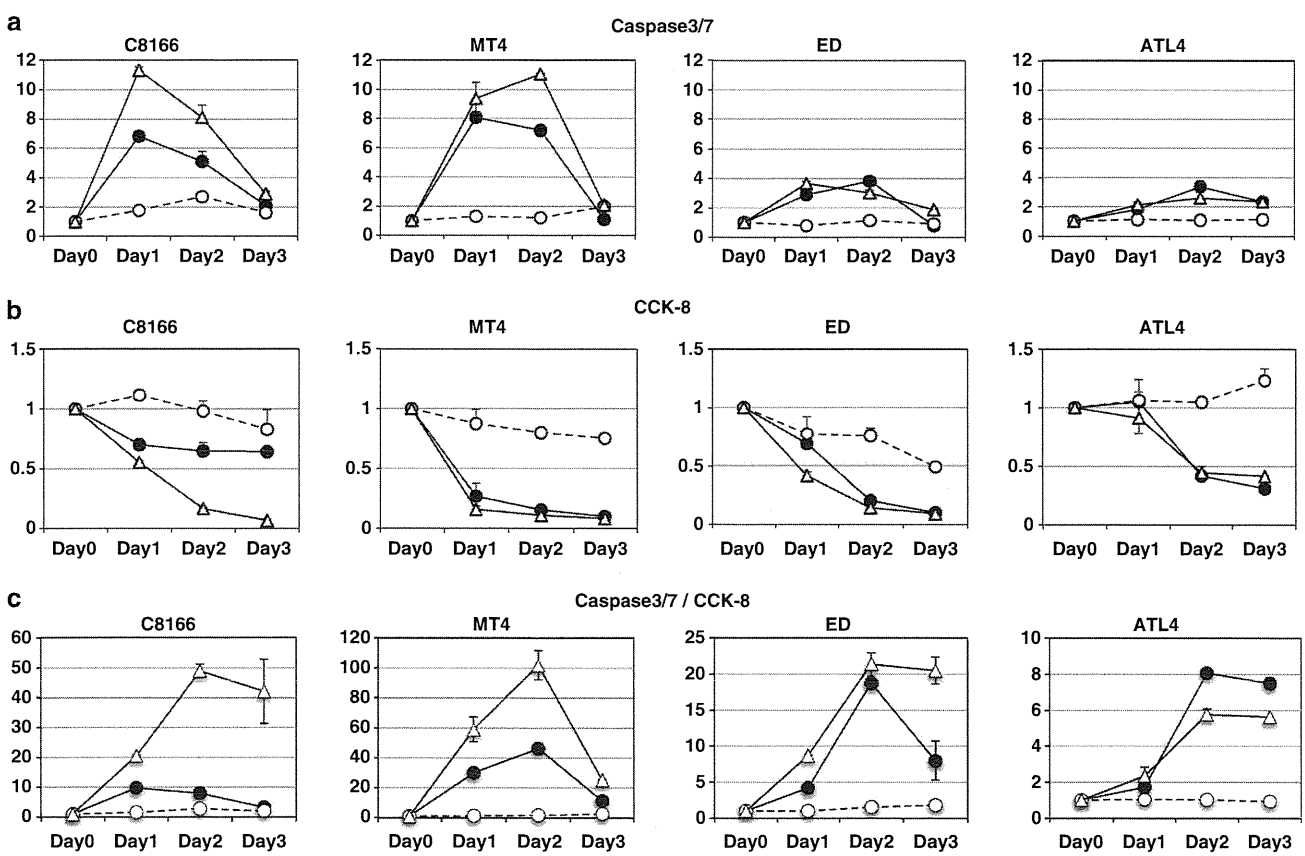

Figure 7. Additive anti-ATL cell effects by the combined dosage of 17-DMAG and Nutlin-3a. (**a**) ATL cell lines C8166, MT4, ED and ATL4 were treated with either suboptimal single dose of 17-DMAG (0.1 μM, black circles) and Nutlin-3a (1 μM, white circles)[41] or both (white triangles) for 3 days and harvested for caspase-3/7 assays (**a**) or CCK-8 assays (**b**) as described in Figure 2. Each untreated cell's value was set as 1. (**c**) Each caspase-3/7 (apoptotic) value was divided by CCK-8 (growth arrest) value to manifest the additive effects (see the Discussion section). CCK-8, Cell Counting Kit 8.

We have determined the therapeutic effects of 17-DMAG on two different ATL model systems through its oral administration. First, we tested 17-DMAG induced prevention of Lck-Tax infiltration in SCID mice, and 5 and 15 mg/kg of oral administration of 17-DMAG for 2 weeks reduced 74% and 83% of Lck-Tax cells, respectively; splenomegaly or massive infiltration of Lck-Tax cells into livers and lungs was also significantly reduced (Figure 5). In all experiments, 17-DMAG mice did not show any body weight losses or inactiveness compared with saline controls.

We then switched to another ATL model experiment JEX/huNOG, which has humanized immune environment in NOG mice and has inoculated HTLV-1-producing Jurkat cells. With oral administration of both 15 and 25 mg/kg 17-DMAG to JEX/huNOG, four of eight mice survived more than 20 weeks, whereas saline controls died within 12 weeks (Figure 6a). 17-DMAG treatment also reduced the number of HTLV-1-infected cells in peripheral blood, suggesting that 17-DMAG treatment could intervene the clonal T-cell development to ATL (Figure 6b). Although this preliminary experiment did not provide statistically significant survival rates, efficacy of this treatment is indeed highly expected. It is necessary to find the optimized conditions suppressing the ATL cell proliferation without any serious side effects.

Tax has pleiotropic effects on intra-cellular or inter-cellular signalings including mitotic checkpoint disruption,[48] aberrant cell-cycle progression[49,50] and altered chemotaxis.[51] The present ATL treatment protocols target the cytoskeletons or DNA replications with multiple doses of anticancer drugs (called as LSG15), and significant side effects by this treatment have been frequently recognized.[40] We have recently demonstrated the potential uses of molecularly targeted inhibitors of ATL cell proliferation, such as a MDM-2 ubiquitin ligase inhibitor Nutlin-3a[41] or CXCR4 antagonist AMD3100.[51] Nutlin-3a induces growth arrest and senescent-cell death of ATL cells at the 10 μM concentration, but normal PBLs are also significantly affected.[41] The combined use of 17-DMAG (0.1 μM) and Nutlin-3a (1 μM), suboptimal concentration for single use, significantly enhanced both apoptotic and growth suppressive effects (Figures 7a and b). This concurrent effects can be manifested with the division of caspase-3/7 values by Cell Counting Kit 8 values (Figure 7c). Besides Nutlin-3a, we also tested the efficacy of 17-DMAG plus LSG15 (without predonisolone; Supplementary Figure 6). Unlike the results of 17-DMAG/Nutlin-3a, 17-DMAG/LSG15 did not show any clear additive effects probably because LSG15 affects cell-cycle progression with a wide range of spectrum, but the effects of Nutlin-3a are specifically restricted to p53 stabilization.

It remains to be seen whether 17-DMAG is effective for ATL patients' treatment; elsewhere Hertlein *et al.*[52] have reported 17-DMAG's clinical application against chronic lymphocytic leukemia. Perhaps in future studies, 17-DMAG and other new drugs with novel anti-ATL activities such as Nutlin-3a, AMD3100 or a monoclonal anti-CCR4 antibody (KW-0761)[53] will provide more effective and less toxic ATL therapy.

CONFLICT OF INTEREST

The authors declare no conflict of interest.

ACKNOWLEDGEMENTS

We are indebted to Dr Herbert C Morse III for his helpful discussion and comments. We thank Mr T Kawashima and Ms Y Itoh for technical assistance and Drs K Terasawa, C Pique and K Nagata for providing plasmid DNAs. EI was a research fellow of the Okinawa Science and Technology Promotion Center. This study was supported in part by grants from the Ministry of Education, Culture, Sports, Science and Technology; the Ministry of Health, Labor and Welfare; the Ministry of Economy, Trade and Industry; Japan Science and Technology Agency; Okinawa Science and Technology Promotion Center; and Miyazaki Prefectural Industrial Support Foundation.

AUTHOR CONTRIBUTIONS

HI, J-IF and HdH designed the research; HdH, HS, WWH, KT, TU and J-IF developed the ATL animal model; EI, AK, KT, ST, SH, TMa, TU, TMi, KS, J-IF, HdH and HI performed the research; AN, MH, HrH, YY, YT, HS, WH, YM, KTJ, MO and KM contributed new reagents/materials; AK, KT, J-IF and HdH contributed pathologic analysis; and EI, KT, J-IF, HdH and HI wrote the paper.

REFERENCES

1 Li Q, Verma IM. NF-kappaB regulation in the immune system. *Nat Rev Immunol* 2002; **2**: 725–734.
2 Janssens S, Tschopp J. Signals from within: the DNA-damage-induced NF-kappaB response. *Cell Death Differ* 2006; **13**: 773–784.
3 Karin M. NF-kappaB as a critical link between inflammation and cancer. *Cold Spring Harb Perspect Biol* 2009; **1**: a000141.
4 Hayden MS, Ghosh S. Shared principles in NF-kappaB signaling. *Cell* 2008; **132**: 344–362.
5 Li XH, Fang X, Gaynor RB. Role of IKK-gamma/NEMO in assembly of the I-kappaB kinase complex. *J Biol Chem* 2001; **276**: 4494–4500.
6 Li Q, Van Antwerp D, Mercurio F, Lee KF, Verma IM. Severe liver degeneration in mice lacking the I-kappaB kinase 2 gene. *Science* 1999; **284**: 321–325.
7 Schmidt-Supprian M, Bloch W, Courtois G, Addicks K, Israel A, Rajewsky K *et al.* NEMO/IKK-gamma-deficient mice model incontinentia pigmenti. *Mol Cell* 2000; **5**: 981–992.
8 Li Q, Lu Q, Hwang JY, Buscher D, Lee KF, Izpisua-Belmonte JC *et al.* IKK1-deficient mice exhibit abnormal development of skin and skeleton. *Genes Dev* 1999; **13**: 1322–1328.
9 Takeda K, Takeuchi O, Tsujimura T, Itami S, Adachi O, Kawai T *et al.* Limb and skin abnormalities in mice lacking IKK-alpha. *Science* 1999; **284**: 313–316.
10 Yamaoka S, Courtois G, Bessia C, Whiteside ST, Weil R, Agou F *et al.* Complementation cloning of NEMO, a component of the I-kappaB kinase complex essential for NF-kappaB activation. *Cell* 1998; **93**: 1231–1240.
11 Iha H, Kibler KV, Yedavalli VR, Peloponese JM, Haller K, Miyazato A *et al.* Segregation of NF-kappaB activation through NEMO/IKK-gamma by Tax and TNF-alpha: implications for stimulus-specific interruption of oncogenic signaling. *Oncogene* 2003; **22**: 8912–8923.
12 Chen G, Cao P, Goeddel DV. TNF-induced recruitment and activation of the IKK complex require Cdc37 and Hsp90. *Mol Cell* 2002; **9**: 401–410.
13 Bouwmeester T, Bauch A, Ruffner H, Angrand PO, Bergamini G, Croughton K *et al.* A physical and functional map of the human TNF-alpha/NF-kappa B signal transduction pathway. *Nat Cell Biol* 2004; **6**: 97–105.
14 Yoshida M. Multiple viral strategies of HTLV-1 for dysregulation of cell growth control. *Annu Rev Immunol* 2001; **19**: 475–496.
15 Hall WW, Fujii M. Deregulation of cell-signaling pathways in HTLV-1 infection. *Oncogene* 2005; **24**: 5965–5975.
16 Matsuoka M, Jeang KT. Human T-cell leukaemia virus type 1 (HTLV-1) infectivity and cellular transformation. *Nat Rev Cancer* 2007; **7**: 270–280.
17 Jin DY, Giordano V, Kibler KV, Nakano H, Jeang KT. Role of adapter function in oncoprotein-mediated activation of NF-kappaB. Human T-cell leukemia virus type I Tax interacts directly with I-kappaB kinase gamma. *J Biol Chem* 1999; **274**: 17402–17405.
18 Carter RS, Pennington KN, Ungurait BJ, Ballard DW. *In vivo* identification of inducible phosphoacceptors in the IKK-gamma/NEMO subunit of human I-kappaB kinase. *J Biol Chem* 2003; **278**: 19642–19648.
19 Lamsoul I, Lodewick J, Lebrun S, Brasseur R, Burny A, Gaynor RB *et al.* Exclusive ubiquitination and sumoylation on overlapping lysine residues mediate NF-kappaB activation by the human T-cell leukemia virus Tax oncoprotein. *Mol Cell Biol* 2005; **25**: 10391–10406.
20 Chu ZL, DiDonato JA, Hawiger J, Ballard DW. The Tax oncoprotein of human T-cell leukemia virus type 1 associates with and persistently activates I-kappaB kinases containing IKK-alpha and IKK-beta. *J Biol Chem* 1998; **273**: 15891–15894.
21 Geleziunas R, Ferrell S, Lin X, Mu Y, Cunningham Jr ET, Grant M *et al.* Human T-cell leukemia virus type 1 Tax induction of NF-kappaB involves activation of the I-kappaB kinase alpha (IKK-alpha) and IKK-beta cellular kinases. *Mol Cell Biol* 1998; **18**: 5157–5165.
22 Egorin MJ, Lagattuta TF, Hamburger DR, Covey JM, White KD, Musser SM *et al.* Pharmacokinetics, tissue distribution, and metabolism of 17-(dimethylaminoethylamino)-17-demethoxygeldanamycin (NSC 707545) in CD2F1 mice and Fischer 344 rats. *Cancer Chemother Pharmacol* 2002; **49**: 7–19.
23 Hasegawa H, Sawa H, Lewis MJ, Orba Y, Sheehy N, Yamamoto Y *et al.* Thymus-derived leukemia–lymphoma in mice transgenic for the Tax gene of human T-lymphotropic virus type I. *Nat Med* 2006; **12**: 466–472.

24 Chiari E, Lamsoul I, Lodewick J, Chopin C, Bex F, Pique C. Stable ubiquitination of human T-cell leukemia virus type 1 tax is required for proteasome binding. *J Virol* 2004; **78**: 11823–11832.
25 Momose F, Naito T, Yano K, Sugimoto S, Morikawa Y, Nagata K. Identification of Hsp90 as a stimulatory host factor involved in influenza virus RNA synthesis. *J Biol Chem* 2002; **277**: 45306–45314.
26 Terasawa K, Minami Y. A client-binding site of Cdc37. *FEBS J* 2005; **272**: 4684–4690.
27 Ueyama T, Kusakabe T, Karasawa S, Kawasaki T, Shimizu A, Son J *et al.* Sequential binding of cytosolic Phox complex to phagosomes through regulated adaptor proteins: evaluation using the novel monomeric Kusabira-Green system and live imaging of phagocytosis. *J Immunol* 2008; **181**: 629–640.
28 Nie C, Sato K, Misawa N, Kitayama H, Fujino H, Hiramatsu H *et al.* Selective infection of CD4+ effector memory T lymphocytes leads to preferential depletion of memory T lymphocytes in R5 HIV-1-infected humanized NOD/SCID/IL-2Rgammanull mice. *Virology* 2009; **394**: 64–72.
29 Ueno S, Umeki K, Takajo I, Nagatomo Y, Kusumoto N, Umekita K *et al.* Proviral loads of human T-lymphotropic virus type 1 in asymptomatic carriers with different infection routes. *Int J Cancer* 2012; **130**: 2318–2326.
30 De Valck D, Jin DY, Heyninck K, Van de Craen M, Contreras R, Fiers W *et al.* The zinc finger protein A20 interacts with a novel anti-apoptotic protein which is cleaved by specific caspases. *Oncogene* 1999; **18**: 4182–4190.
31 Peloponese JM, Iha H, Yedavalli VR, Miyazato A, Li Y, Haller K *et al.* Ubiquitination of human T-cell leukemia virus type 1 tax modulates its activity. *J Virol* 2005; **78**: 11686–11695.
32 Yan P, Qing G, Qu Z, Wu CC, Rabson A, Xiao G. Targeting autophagic regulation of NFkappaB in HTLV-I transformed cells by geldanamycin: implications for therapeutic interventions. *Autophagy* 2007; **3**: 600–603.
33 Mitsiades CS, Mitsiades NS, McMullan CJ, Poulaki V, Kung AL, Davies FE *et al.* Antimyeloma activity of heat shock protein-90 inhibition. *Blood* 2006; **107**: 1092–1100.
34 Jeang KT, Chiu R, Santos E, Kim SJ. Induction of the HTLV-I LTR by Jun occurs through the Tax-responsive 21-bp elements. *Virology* 1991; **181**: 218–227.
35 Prodromou C, Roe SM, O'Brien R, Ladbury JE, Piper PW, Pearl LH. Identification and structural characterization of the ATP/ADP-binding site in the Hsp90 molecular chaperone. *Cell* 1997; **90**: 65–75.
36 Meyer P, Prodromou C, Hu B, Vaughan C, Roe SM, Panaretou B *et al.* Structural and functional analysis of the middle segment of hsp90: implications for ATP hydrolysis and client protein and cochaperone interactions. *Mol Cell* 2003; **11**: 647–658.
37 Minami Y, Kimura Y, Kawasaki H, Suzuki K, Yahara I. The carboxy-terminal region of mammalian HSP90 is required for its dimerization and function *in vivo*. *Mol Cell Biol* 1994; **14**: 1459–1464.
38 Roe SM, Ali MM, Meyer P, Vaughan CK, Panaretou B, Piper PW *et al.* The mechanism of Hsp90 regulation by the protein kinase-specific cochaperone p50(cdc37). *Cell* 2004; **116**: 87–98.
39 Silverstein AM, Grammatikakis N, Cochran BH, Chinkers M, Pratt WB. p50(cdc37) binds directly to the catalytic domain of Raf as well as to a site on hsp90 that is topologically adjacent to the tetratricopeptide repeat binding site. *J Biol Chem* 1998; **273**: 20090–20095.
40 Uozumi K. Treatment of adult T-cell leukemia. *J Clin Exp Hematop* 2010; **50**: 9–25.
41 Hasegawa H, Yamada Y, Iha H, Tsukasaki K, Nagai K, Atogami S *et al.* Activation of p53 by Nutlin-3a, an antagonist of MDM2, induces apoptosis and cellular senescence in adult T-cell leukemia cells. *Leukemia* 2009; **23**: 2090–2101.
42 Proietti FA, Carneiro-Proietti AB, Catalan-Soares BC, Murphy EL. Global epidemiology of HTLV-I infection and associated diseases. *Oncogene* 2005; **24**: 6058–6068.
43 Mizushima N, Yoshimori T, Ohsumi Y. The role of Atg proteins in autophagosome formation. *Annu Rev Cell Dev Biol* 2011; **27**: 107–132.
44 Codogno P, Mehrpour M, Proikas-Cezanne T. Canonical and non-canonical autophagy: variations on a common theme of self-eating? *Nat Rev Mol Cell Biol* 2011; **13**: 7–12.
45 Terasawa K, Yoshimatsu K, Iemura SI, Natsume T, Tanaka K, Minami Y. Cdc37 interacts with the glycine-rich loop of Hsp90 client kinases. *Mol Cell Biol* 2006; **26**: 3378–3389.
46 Calderwood SK, Khaleque MA, Sawyer DB, Ciocca DR. Heat shock proteins in cancer: chaperones of tumorigenesis. *Trends Biochem Sci* 2006; **31**: 164–172.
47 Caplan AJ, Mandal AK, Theodoraki MA. Molecular chaperones and protein kinase quality control. *Trends Cell Biol* 2007; **17**: 87–92.
48 Jin DY, Spencer F, Jeang KT. Human T cell leukemia virus type 1 oncoprotein Tax targets the human mitotic checkpoint protein MAD1. *Cell* 1998; **93**: 81–91.
49 Giam CZ, Jeang KT. HTLV-1 Tax and adult T-cell leukemia. *Front Biosci* 2007; **12**: 1496–1507.
50 Tanaka Y. Activation of leukocyte function-associated antigen-1 on adult T-cell leukemia cells. *Leuk Lymphoma* 1999; **36**: 15–23.
51 Kawaguchi A, Orba Y, Kimura T, Iha H, Ogata M, Tsuji T *et al.* Inhibition of the SDF-1alpha-CXCR4 axis by the CXCR4 antagonist AMD3100 suppresses the migration of cultured cells from ATL patients and murine lymphoblastoid cells from HTLV-I Tax transgenic mice. *Blood* 2009; **114**: 2961–2968.
52 Hertlein E, Wagner AJ, Jones J, Lin TS, Maddocks KJ, Towns III WH *et al.* 17-DMAG targets the nuclear factor-kappaB family of proteins to induce apoptosis in chronic lymphocytic leukemia: clinical implications of HSP90 inhibition. *Blood* 2010; **116**: 45–53.
53 Yamamoto K, Utsunomiya A, Tobinai K, Tsukasaki K, Uike N, Uozumi K *et al.* Phase I study of KW-0761, a defucosylated humanized anti-CCR4 antibody, in relapsed patients with adult T-cell leukemia–lymphoma and peripheral T-cell lymphoma. *J Clin Oncol* 2010; **28**: 1591–1598.

Supplementary Information accompanies this paper on the Blood Cancer Journal website (http://www.nature.com/bcj).